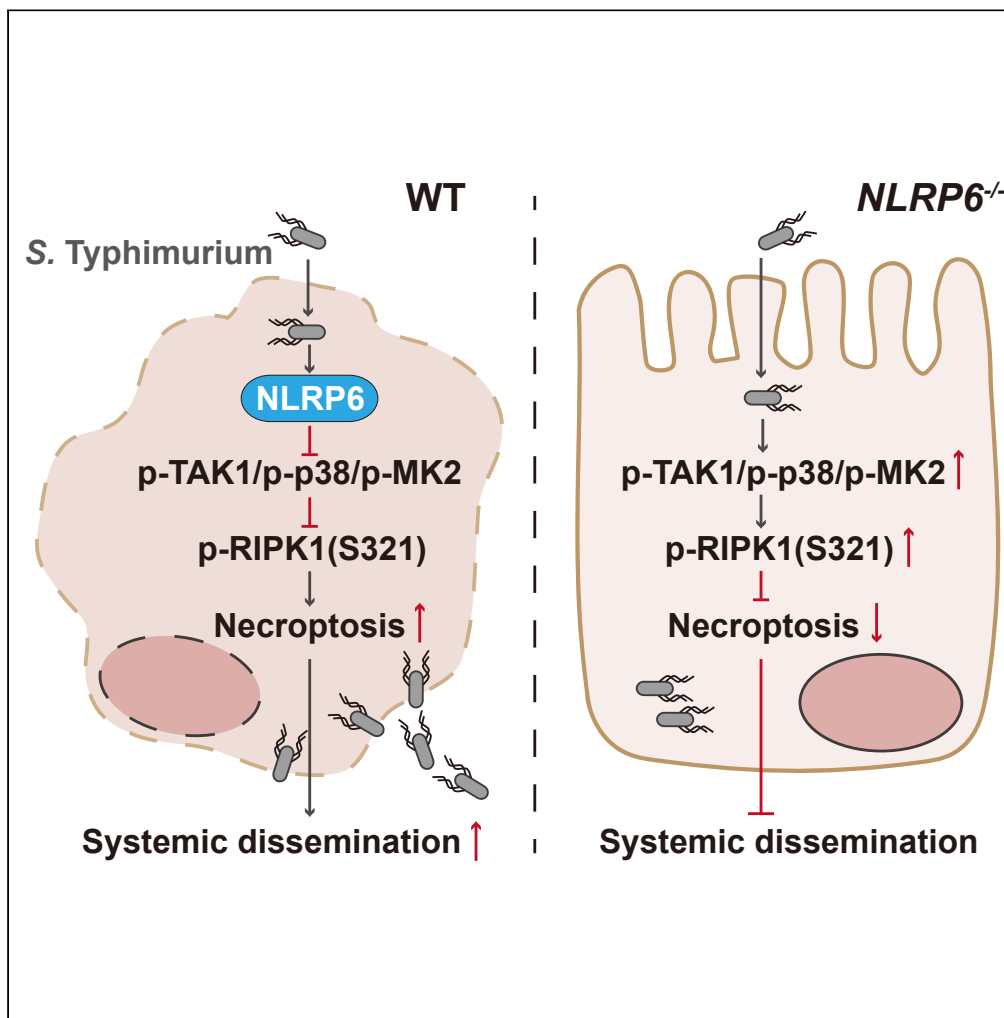


Article

NLRP6 induces RIP1 kinase-dependent necroptosis via TAK1-mediated p38^{MAPK}/MK2 phosphorylation in *S. typhimurium* infection

Qifeng Deng, Sidi Yang, Kai Huang, ..., Yuanyuan Li, Shuyan Wu, Rui Huang

liyuan@suda.edu.cn (Y.L.)
wushuyan@suda.edu.cn (S.W.)
hruisdm@163.com (R.H.)

Highlights

NLRP6 promotes *S. typhimurium*-induced necroptosis in a RIP1 dependent manner

NLRP6 decreases phosphorylation of RIP1 at S321 via the TAK1-p38MAPK-MK2 pathway

NLRP6 deficiency is benefit for controlling *S. typhimurium* dissemination

Deng et al., iScience 27, 109339
April 19, 2024 © 2024 The Author(s).
<https://doi.org/10.1016/j.isci.2024.109339>

Article

NLRP6 induces RIP1 kinase-dependent necroptosis via TAK1-mediated p38^{MAPK}/MK2 phosphorylation in *S. typhimurium* infectionQifeng Deng,^{1,2,9} Sidi Yang,^{3,9} Kai Huang,^{4,9} Yuan Zhu,^{1,5} Lanqing Sun,^{1,6} Yu Cao,¹ Kedi Dong,^{1,7} Yuanyuan Li,^{8,*} Shuyan Wu,^{1,*} and Rui Huang^{1,10,*}

SUMMARY

Programmed cell death (PCD) is tightly orchestrated by molecularly defined executors and signaling pathways. NLRP6, a member of cytoplasmic pattern recognition receptors, has a multifaceted role in host resistance to bacterial infection. However, whether and how NLRP6 may contribute to regulate host PCD during Gram-negative bacterial infection remain to be illuminated. Here, we report that NLRP6 promotes RIP1 kinase-mediated necroptosis, a form of lytic PCD, in both an *in vitro* and *in vivo* model of *Salmonella typhimurium* infection. By downregulating TAK1-mediated p38^{MAPK}/MK2 phosphorylation, NLRP6 decreased RIP1 phosphorylation at residue S321 and subsequently increased RIP1 kinase-dependent MLKL phosphorylation. Suppression of p38^{MAPK}/MK2 cascade not only reduced the number of dead cells caused by NLRP6 but also decreased the systemic dissemination of *S. typhimurium* resulting from NLRP6. Taken together, our findings provide new insights into the role and regulatory mechanism of NLRP6-associated antimicrobial responses by revealing a function for NLRP6 in regulating necroptosis.

INTRODUCTION

Necroptosis, a modality of programmed cell death (PCD) first described in 2005,¹ has important functions in host antimicrobial defense and inflammation.² The serine/threonine kinase RIP1 (receptor interacting protein kinase-1) is identified as a central mediator of necroptosis, and its activity is tightly controlled by phosphorylation modification. When subjected to either extrinsic or intrinsic driving factors, cells initiate the assembly of a cell death platform containing RIP1 and receptor interacting protein kinase-3 (RIP3), termed necrosome.³ RIP3 subsequently recruits and mediates phosphorylation of its substrate mixed lineage kinase domain-like pseudokinase (MLKL), leading to MLKL translocation from the cytoplasm to the plasma membrane and induction of membrane damage.⁴ MLKL serves as the necroptotic executioner to initiate lytic cell death, which not only increases the release of damage-associated molecular patterns (DAMPs) such as ATP and high-mobility group box 1 (HMGB1) but also triggers the inflammatory response and cell death mechanism in surrounding cells.⁵

NLRP6, a recently discovered member of the nucleotide-oligomerization domain-like receptors (NLRs), is present in the cytosol of both myeloid and intestinal epithelial cells, acting as a crucial regulator involved in maintaining intestinal homeostasis and orchestrating immune responses.^{6,7} NLRP6 recruits the adaptor protein ASC to form an inflammasome complex with caspase-1 and caspase-11, resulting in processing pro-interleukin-1 β (pro-IL-1 β) and -18 (pro-IL-18) into their mature form.⁸ Unlike other NLRs, NLRP6 is also capable of regulating inflammatory signaling and impeding bacterial clearance in an inflammasome-independent manner.⁹ An interesting study by Ghimire et al. reported that NLRP6-deficient macrophages showed reduced necroptosis following Gram-positive bacterial infection.¹⁰ However, detailed signaling mechanisms of how NLRP6 induced cell death by necroptosis have not been explored. In addition, whether NLRP6 is associated with necroptosis in response to Gram-negative bacterial infection remains elusive.

Salmonella enterica serovar *typhimurium* (*S. typhimurium*) is one of the most common Gram-negative facultative intracellular bacterium that has long been used as a model for investigating the interaction between enteropathogenic bacteria and the host.^{11,12} Previous studies

¹Department of Medical Microbiology, MOE Key Laboratory of Geriatric Diseases and Immunology, Suzhou Key Laboratory of Pathogen Bioscience and Anti-infective Medicine, School of Biology & Basic Medical Sciences, Suzhou Medical College of Soochow University, Suzhou, Jiangsu 215123, P.R. China

²MOE Key Laboratory of Gene Function and Regulation, State Key Laboratory of Biocontrol, School of Life Sciences, Sun Yat-sen University, Guangzhou, Guangdong 510275, P.R. China

³Guangzhou National Laboratory, Guangzhou International Bio Island, Guangzhou, Guangdong 510005, P.R. China

⁴Orthopaedic Institute, Wuxi 9th People's Hospital Affiliated to Soochow University, Wuxi, Jiangsu 214062, P.R. China

⁵Department of Laboratory Medicine, The First Affiliated Hospital of Ningbo University, Ningbo, Zhejiang 315010, P.R. China

⁶Department of Laboratory Medicine, Affiliated Hospital of Jiangnan University, Wuxi, Jiangsu 214000, P.R. China

⁷Department of Blood Transfusion, The First Affiliated Hospital of Ningbo University, Ningbo, Zhejiang 315010, P.R. China

⁸Experimental Center, Suzhou Medical College of Soochow University, No. 199, Ren Ai Road, Suzhou, Jiangsu 215123, P.R. China

⁹These authors contributed equally

¹⁰Lead contact

*Correspondence: liyuanyuan@suda.edu.cn (Y.L.), wushuyan@suda.edu.cn (S.W.), hruidm@163.com (R.H.)

<https://doi.org/10.1016/j.isci.2024.109339>



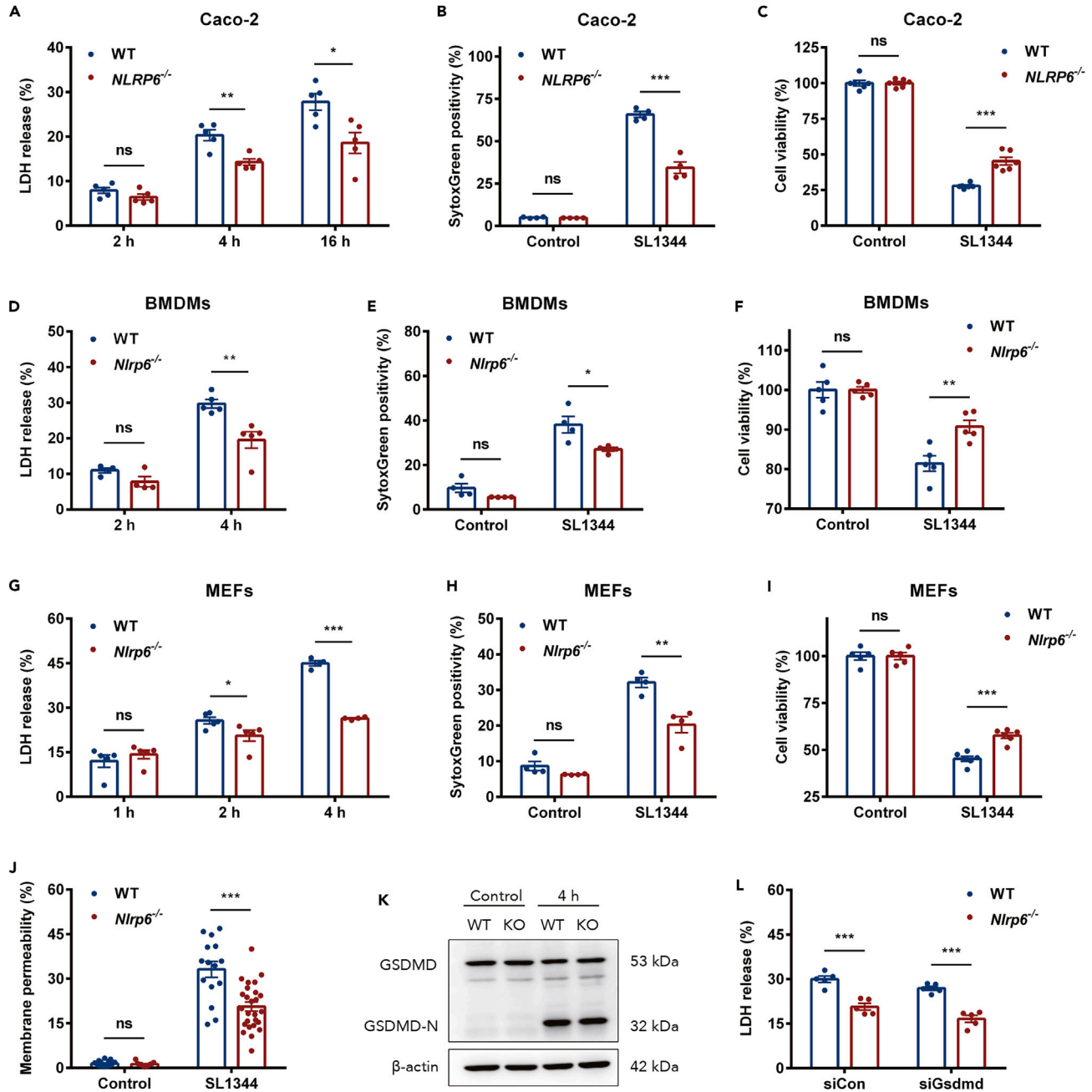


Figure 1. NLRP6 deficiency decreases *S. typhimurium*-induced cell death

(A) Cell death kinetics analyzed by LDH release in WT and *NLRP6*^{-/-} Caco-2 cells infected with *S. typhimurium* strain SL1344 at an MOI of ~100 for the indicated time points.

(B) Cell death assayed by Sytox Green staining in WT and *NLRP6*^{-/-} Caco-2 cells infected with SL1344 at an MOI of ~100 for 16 h.

(C) Cell viability of WT and *NLRP6*^{-/-} Caco-2 cells infected with SL1344 at an MOI of ~100 for 16 h.

(D) Cell death kinetics analyzed by LDH release of WT and *Nlrp6*^{-/-} BMDMs infected with SL1344 at an MOI of 20 for the indicated time points.

(E) Cell death assayed by Sytox Green staining of WT and *Nlrp6*^{-/-} BMDMs infected with SL1344 at an MOI of 20 for 4 h.

(F) Cell viability of WT and *Nlrp6*^{-/-} BMDMs infected with SL1344 at an MOI of 20 for 4 h.

(G) Cell death kinetics analyzed by LDH release of WT and *Nlrp6*^{-/-} MEFs infected with SL1344 at an MOI of 10 for the indicated time points.

(H) Cell death assayed by Sytox Green staining of WT and *Nlrp6*^{-/-} MEFs infected with SL1344 at an MOI of 10 for 4 h.

(I) Cell viability of MEFs of WT and *Nlrp6*^{-/-} MEFs infected with SL1344 at an MOI of 10 for 4 h.

Figure 1. Continued

(J) Membrane permeability of WT and *Nlrp6*^{-/-} BMDMs infected with SL1344 at an MOI of 20 for 4 h. (n > 1000 cells per group).

(K) Western blot analysis of WT and *Nlrp6*^{-/-} MEFs infected with SL1344 at an MOI of 10 for 4 h.

(L) Cell death assayed by LDH release of WT and *Nlrp6*^{-/-} MEFs transfected with 50 nM either negative-control siRNA or *Gsdmd*-specific siRNA for 48 h, followed by infection with SL1344 at an MOI of 10 for 4 h. Data were compared with independent Student's t test. Values are expressed as the mean ± SEM, and statistically significant differences are indicated. *p < 0.05; **p < 0.01; ***p < 0.001; ns, not significant.

have shown that host PCD is a crucial immune defense mechanism in response to bacterial infection.¹³ For instance, the sacrifice of infected cells, such as the expulsion of epithelial cells containing *S. typhimurium*, is required for removing replicative niches for intracellular bacteria and preventing its negative influence on the remaining healthy cells.¹⁴ However, cell death is a double-edged sword, which also has benefits for bacterial pathogens. By manipulating the death of infected cells, *S. typhimurium* crosses the intestinal barrier and escapes from immune cells to maintain their nutrient requirement and promote their pathogenesis.¹⁵ Inhibition of necroptosis, therefore, is beneficial to ameliorating inflammatory damage, limiting pathogen spread, and promoting host survival during *S. typhimurium* infection.^{16–18} Our recent study has reported that NLRP6 facilitated *S. typhimurium* intracellular replication by regulating host iron metabolism.¹⁹ In the current study, we further reveal a detrimental role of NLRP6 in promoting *S. typhimurium* systemic dissemination. Our results identify potential interconnection between NLRP6 and RIP1 kinase-dependent necroptosis during *S. typhimurium* infection, and suggest NLRP6 as a therapeutic target for limiting enteropathogenic bacteria systemic dissemination.

RESULTS**NLRP6 enhances *S. typhimurium*-associated cell death via a pyroptosis-independent pathway**

As a typical foodborne pathogen, *S. typhimurium* infection usually occurs through the oral route and first invades the intestinal epithelial cells (IECs). Once crossing the intestinal barrier, *S. typhimurium* is captured by phagocytes such as macrophages and further disseminates to systemic organs.²⁰ To explore whether NLRP6 is involved in host cell death during *S. typhimurium* infection, wild-type (WT) and NLRP6 knockout (*NLRP6*^{-/-}) human Caco-2 IEC lines were used to establish an *in vitro* model of *S. typhimurium* infection. There was no significant difference in the percentage of dead cells between *S. typhimurium*-infected WT and *NLRP6*^{-/-} Caco-2 cells at 2 h post-infection, whereas *NLRP6*^{-/-} Caco-2 cells displayed a significantly lower ratio of dead to normal cells when compared to WT Caco-2 cells at 4 and 16 h post-infection (Figures 1A and 1B). As a complementary approach, we also conducted studies detecting the cell viability. As shown in Figure 1C, the percentage of viable cells was significantly higher in *NLRP6*^{-/-} than in WT Caco-2 cells after infection. To further decipher the role of NLRP6 in phagocyte cell death during *S. typhimurium* infection, we conducted studies using bone marrow-derived macrophages (BMDMs) isolated from WT or *Nlrp6*^{-/-} mice. In line with the results obtained in IECs, the infected *Nlrp6*^{-/-} BMDMs exhibited a significant higher cell viability when compared with their WT counterparts (Figures 1D–1F). Given that mouse embryonic fibroblasts (MEFs) are an ideal tool for studying PCD and convenient for intervention experiments, we further performed *in vitro* infection experiments using MEFs isolated from WT or *Nlrp6*^{-/-} mice. Consistent with the above observation, NLRP6 deficiency decreased cell death in MEFs during infection (Figures 1G–1I).

A recent study reported that, during Gram-positive bacterial infection, NLRP6 promotes pyroptosis-associated cell lysis via assembling the NLRP6-ASC-caspase1/11 inflammasome complex and subsequent cleavage of the pyroptosis execution protein gasdermin D (GSDMD).¹⁰ Therefore, we wondered whether NLRP6 had a role in promoting pyroptosis during Gram-negative bacterial infection. Our data showed NLRP6 deficiency dramatically reduced membrane permeability in *S. typhimurium*-infected cells (Figure 1J), suggesting that NLRP6-associated cell death is accompanied by plasma membrane rupture. To our surprise, immunofluorescence analysis showed that *S. typhimurium* infection led to an increase of both NLRP6 and ASC within the cytoplasm of the Caco-2 cells, while we did not observe NLRP6 co-localize with ASC (Figure S1A). Importantly, loss of NLRP6 had no significant effect on *S. typhimurium*-induced cleavage of GSDMD in MEFs, Caco-2 cells and BMDMs (Figures 1K, S1B, and S2A). Knockdown of *Gsdmd* in MEFs using a small interfering RNA (siRNA) could not reverse the effect of NLRP6 deficiency on cell death (Figure 1L). In line with these findings, there was no significant difference in the cleavage-activation of either caspase-1 or caspase-4/11 and the release of IL-1β between *S. typhimurium*-infected WT and NLRP6 knockout cells (Figures S1C–S1I and S2B–S2F). These findings suggest that NLRP6 facilitates cell death during *S. typhimurium* infection. However, this phenomenon is independent of inflammasome-mediated pyroptosis.

NLRP6 promotes necroptosis in a RIP1 kinase-dependent manner during *S. typhimurium* infection

Necroptosis and pyroptosis are two of the most common types of PCD associated with plasma membrane pore formation.²¹ To investigate the contribution of NLRP6 to *S. typhimurium*-relevant necroptosis, the MLKL inhibitor GW806742X was used and the phosphorylation level of MLKL measured. Treatment with GW806742X reduced *S. typhimurium*-induced cell death and abolished the significant difference in the number of dead cells between WT and *Nlrp6*^{-/-} MEFs (Figure 2A). Of note, the level of MLKL phosphorylation was significantly lower in *Nlrp6*^{-/-} than in WT MEFs (Figure 2B), suggesting that NLRP6 mediates the induction of necroptosis during *S. typhimurium* infection. RIP1 is an upstream kinase that interacts with RIP3 and subsequently mediates the formation of RIP3-MLKL complexes, resulting in necroptosis induction. However, RIP3 can also induce necroptosis independently of RIP1.^{22,23} Our data showed that treatment with the RIP3 inhibitor GSK'872 reduced *S. typhimurium*-induced cell death and reversed the significant difference in the number of dead cells between WT and *Nlrp6*^{-/-} MEFs (Figure 2C). HeLa cells, a RIP3-deficient cell line, were transfected with the HA-tagged RIP3 plasmid for establishing a non-pharmacological model.²⁴ We found a significantly higher percentage of cell death in HeLa cells co-expressing RIP3 and NLRP6 when

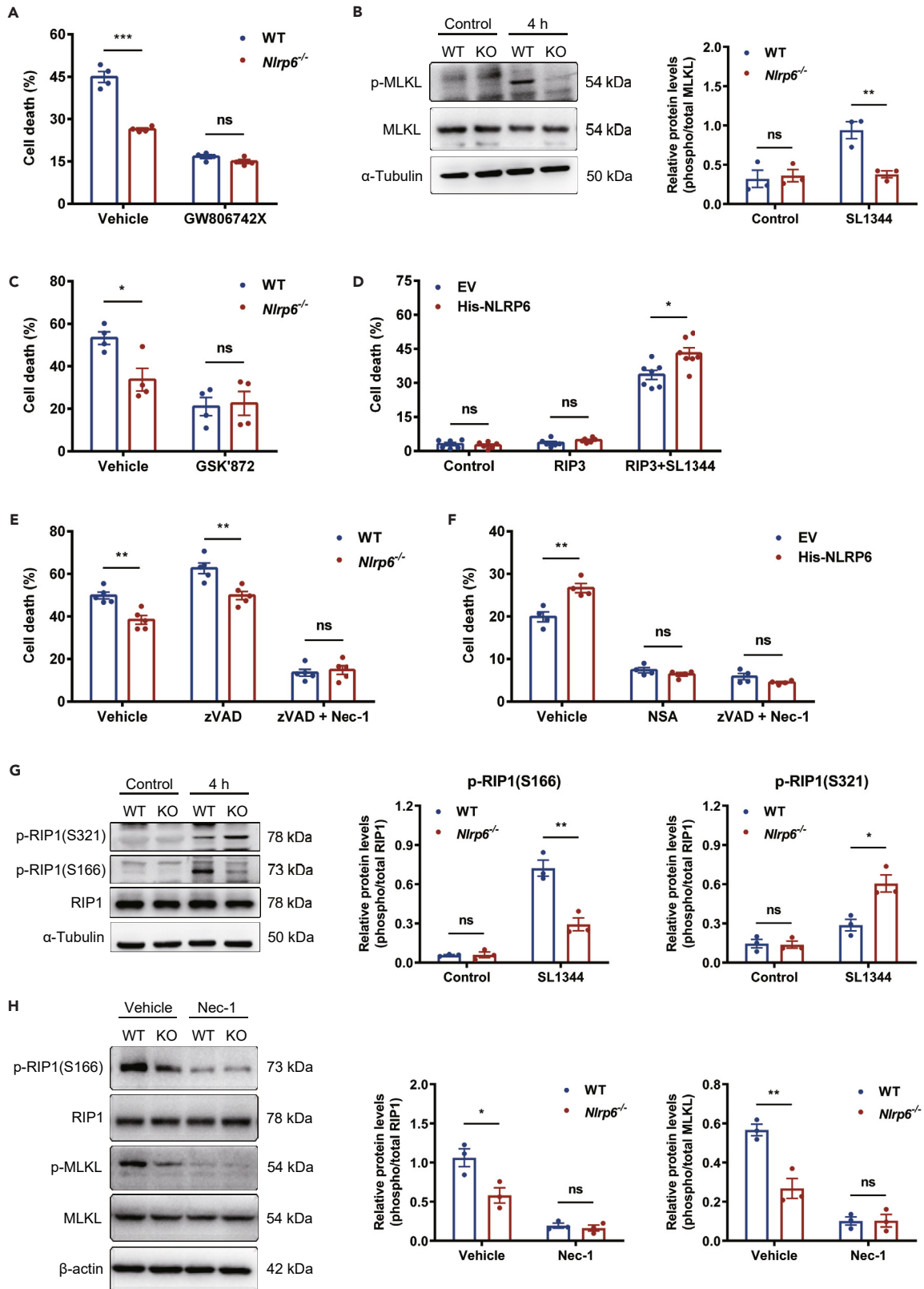


Figure 2. NLRP6 deficiency decreases *S. typhimurium*-induced necroptosis in a RIP1 kinase-dependent manner

(A) Cell death of WT and *Nlrp6*^{-/-} MEFs treated with either vehicle or the MLKL inhibitor GW806742X for 1 h, followed by infection with *S. typhimurium* strain SL1344 at an MOI of 10 for 4 h.

(B) Western blot analysis and relative intensity of WT and *Nlrp6*^{-/-} MEFs infected with SL1344 at an MOI of 10 for 4 h.

(C) Cell death of WT and *Nlrp6*^{-/-} MEFs treated with either vehicle or the RIP3 inhibitor GSK872 for 1 h, followed by infection with SL1344 at an MOI of 10 for 4 h.

(D) Cell death of HeLa cells transfected with plasmids encoding His-NLRP6 together with HA-RIP3, followed by infection with SL1344 at an MOI of 100 for 4 h.

(E) Cell death of WT and *Nlrp6*^{-/-} MEFs treated with vehicle, the pan-caspase inhibitor zVAD or the RIP1 inhibitor Nec-1 along with zVAD for 1 h, followed by infection with SL1344 at an MOI of 10 for 4 h.

(F) Cell death of HeLa cells transfected with plasmids encoding His-NLRP6 together with HA-RIP3, after treated with vehicle, NSA or zVAD+Nec-1 for 1 h, followed by infection with SL1344 at an MOI of 100 for 4 h.

(G) Western blot analysis and relative intensity of WT and *Nlrp6*^{-/-} MEFs infected with SL1344 at an MOI of 10 for 4 h.

(H) Western blot analysis and relative intensity of WT and *Nlrp6*^{-/-} MEFs treated with either vehicle or the RIP1 inhibitor Nec-1 for 1 h, followed by infection with SL1344 at an MOI of 10 for 4 h. Data were compared with independent Student's t test. Values are expressed as the mean ± SEM, and statistically significant differences are indicated. All data are representative of at least three independent experiments. *p < 0.05; **p < 0.01; ***p < 0.001; ns, not significant.

compared to the control group during infection (Figure 2D). To further examine whether RIP1 is involved in NLRP6-mediated necroptosis, cells were treated with the RIP1 inhibitor necrostatin-1 (Nec-1) with or without the pan-caspase inhibitor zVAD as previously described.²⁵ Although the percentage of cell death was still lower in *Nlrp6*^{-/-} than in WT MEFs after administering zVAD, treatment with Nec-1 + zVAD not only reduced cell death but also reversed the apparent difference between the infected MEFs of these two genotypes (Figure 2E). Concomitantly, treatment of RIP3-expressed HeLa cells with either the MLKL inhibitor necrosulfonamide (NSA) or Nec-1 + zVAD abrogated the significant difference in the number of dead cells caused by NLRP6 (Figure 2F). We also found that phosphorylation of RIP1 at S166—a biomarker tightly associated with the activation of RIP1 and the initiation of necroptosis—was significantly lower in *Nlrp6*^{-/-} than in WT MEFs following *S. typhimurium* infection (Figure 2G). Meanwhile, a higher phosphorylated level of RIP1 at S321, a residue that inhibits RIP1 kinase activity, was observed in *Nlrp6*^{-/-} MEFs compared with WT MEFs (Figure 2G). Importantly, treatment of *S. typhimurium*-infected cells with the RIP1 inhibitor abolished the apparent difference in the phosphorylation level of RIP1(S166) and MLKL between these two genotypes during infection (Figure 2H). These observations collectively indicate that NLRP6 facilitates necroptosis during *S. typhimurium* infection through modulating RIP1 kinase activity and the subsequent cascade of RIP1-RIP3-MLKL.

NLRP6 influences phosphorylation of RIP1 at S321 via the TAK1-p38^{MAPK}-MK2 signaling cascade

We next focused on elucidating the mechanisms underlying NLRP6-initiated necroptosis and the pathway whereby NLRP6 could regulate RIP1 phosphorylation at S321 in response to Gram-negative bacterial infection. It has been reported that NLRP6 dampens nuclear factor Kappa-B (NF-κB) activation.⁹ Therefore, we first sought to explore whether this pathway contributes to NLRP6-associated necroptosis. In line with the results obtained in the hematopoietic cells, our data showed that NLRP6 downregulated the kinetics of IκBα degradation in *S. typhimurium*-infected MEFs (Figure S3A), suggesting that NLRP6 could also inhibit NF-κB activity in non-hematopoietic cells. The activation of NF-κB can be triggered by various exogenous and endogenous stimuli such as interleukin-1β (IL1β), tumor necrosis factor (TNFα), or phorbol myristate acetate (PMA).²⁶ We found that either NF-κB activation or IκBα degradation induced by one of three agonists was suppressed by NLRP6 overexpression (Figures S3B–S3E). We further sought to identify where in the NF-κB signaling pathway NLRP6 might exert its inhibitory function. Overexpression of NLRP6 reduced NF-κB activity stimulated with both TNF-receptor associated factor 2 (TRAF2), the crucial downstream ligase of TNFα receptor, and TRAF6, the key downstream mediator of IL1β receptor. However, overexpression of NLRP6 had no inhibitory effect on the activation of NF-κB induced by TGF-β-activated kinase 1 (TAK1), inhibitor of nuclear factor-κB kinase β (IKKβ), and p65 (Figures S3F), suggesting that NLRP6 functioned at the level of the TAK1, which is an essential modulator that provides a vital link downstream of TRAF to upstream of IKK. We presume that TAK1 is involved not only in NLRP6-mediated NF-κB inhibition but also in NLRP6-associated necroptosis induction. Consistent with our hypothesis, treatment of *S. typhimurium*-infected MEFs with the inhibitor of TAK1 catalytic activity reversed the significant difference in cell death between WT and *Nlrp6*^{-/-} cells (Figure S3G).

We subsequently sought to determine the mechanism by which NLRP6 regulates TAK1-associated necroptosis. Our data showed that overexpression of NLRP6 had slight influence on the protein level of TAK1 (Figure 3A). We also treated cells with the protein synthesis inhibitor cycloheximide (CHX) to assess whether NLRP6 influences the stability of TAK1 protein and observed the degradation rate of TAK1 in WT cells was similar to that of *Nlrp6*^{-/-} cells (Figure 3B). These data suggested that NLRP6 may regulate the kinase activity of TAK1 but not the expression of TAK1. In line with our hypothesis, no apparent difference in the protein level of TAK1 was observed between *S. typhimurium*-infected WT and *Nlrp6*^{-/-} cells, while a significantly higher phosphorylated level of TAK1 was observed in *Nlrp6*^{-/-} than in WT MEFs (Figure 3C). TAK1 phosphorylation and activation were found to be closely related to its ubiquitination.^{27,28} Our data supported these previous observations showing that NLRP6 interacted with TAK1 and *Nlrp6*^{-/-} cells displayed a dramatically higher level of ubiquitinated TAK1 when compared to WT cells during *S. typhimurium* infection (Figures 3D and 3E). The p38 Mitogen-activated protein kinase (p38^{MAPK}) is identified as one of the several downstream kinases that are regulated by TAK1 phosphorylation. Through phosphorylation of a direct downstream substrate MAPK-activated protein kinase 2 (MK2), the p38^{MAPK}-MK2 axis phosphorylates RIP1 at S321 to prevent necroptosis in inflammation and infection.²⁹ We presumed that the p38^{MAPK}/MK2 pathway has a potential role in NLRP6-induced TAK1-dependent necroptosis. Loss of NLRP6 had no significant effect on p38^{MAPK} and MK2 expression. However, treatment with the p38^{MAPK} inhibitor SB239063 increased *S. typhimurium*-induced cell death and abrogated the significant difference in the number of dead cells between WT

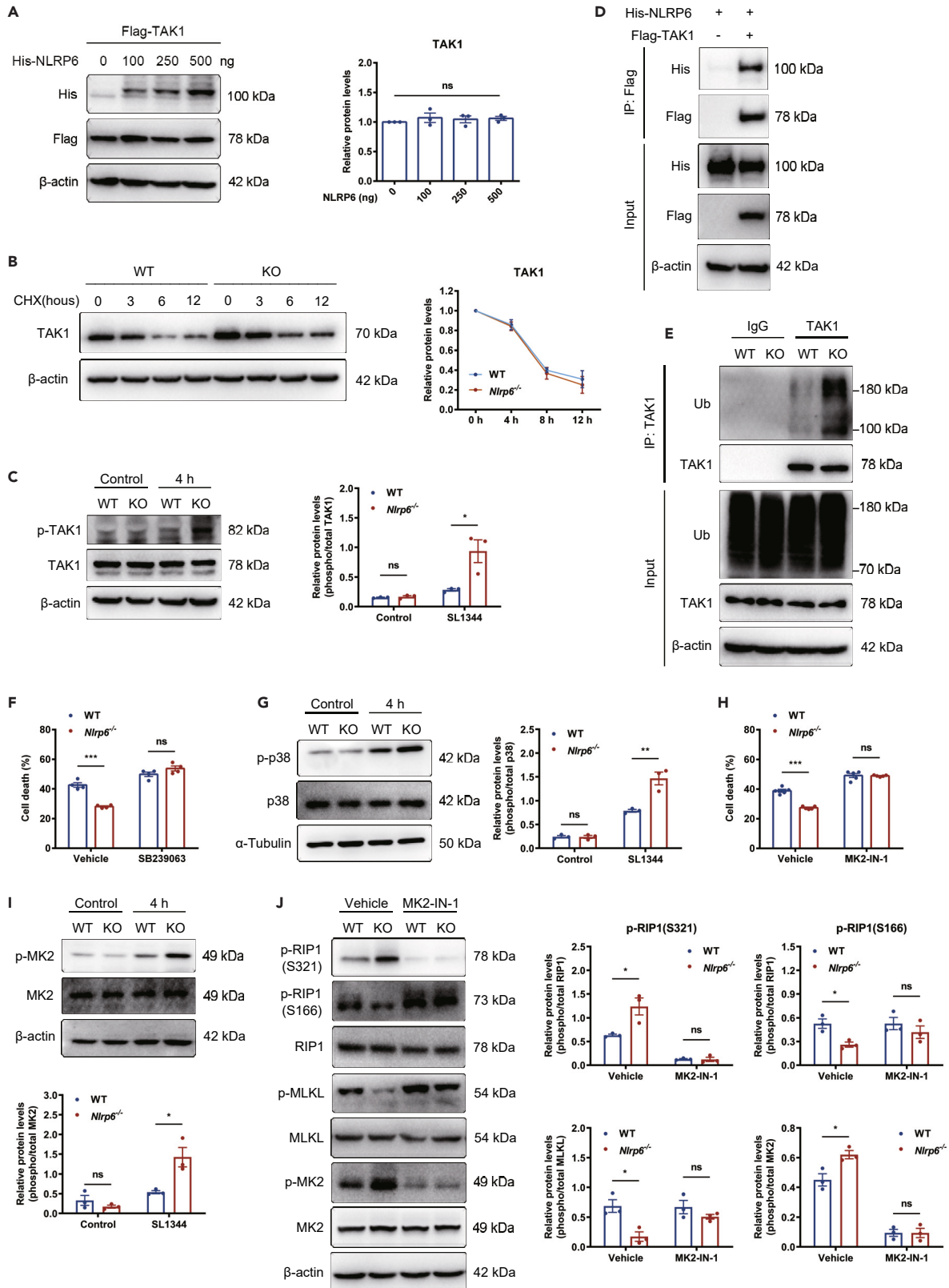


Figure 3. NLRP6 deficiency increases RIP1 phosphorylation at S321 via the TAK1/p38^{MAPK}/MK2 cascade

- (A) Western blot analysis and relative intensity of HEK293T cells transfected with plasmids encoding His-NLRP6 together with HA-RIP3 indicated concentration of Flag-TAK1.
- (B) Western blot analysis and relative intensity of WT and *Nlrp6*^{-/-} MEFs treated with the protein synthesis inhibitor CHX for indicated time points.
- (C) Western blot analysis and relative intensity of WT and *Nlrp6*^{-/-} MEFs infected with *S. typhimurium* strain SL1344 at an MOI of 10 for 4 h.
- (D) Immunoblot analysis of whole-cell lysates of 293T cells transfected with plasmids encoding His-NLRP6 and Flag-TAK1, followed by immunoprecipitation with anti-Flag beads.
- (E) Western blot analysis of protein extracts of WT and *Nlrp6*^{-/-} MEFs infected with SL1344 at an MOI of 10 for 4 h, followed by immunoprecipitation with anti-TAK1 antibody.
- (F) Cell death of WT and *Nlrp6*^{-/-} MEFs treated with either vehicle or the p38^{MAPK} inhibitor SB239063 for 30 min, followed by infection with SL1344 at an MOI of 10 for 4 h.
- (G) Western blot analysis and relative intensity of WT and *Nlrp6*^{-/-} MEFs infected with SL1344 at an MOI of 10 for 4 h.
- (H) Cell death of WT and *Nlrp6*^{-/-} MEFs treated with either vehicle or the MK-2 inhibitor MK2-IN-1 for 30 min, followed by infection with SL1344 at an MOI of 10 for 4 h.
- (I) Western blot analysis and relative intensity of WT and *Nlrp6*^{-/-} MEFs infected with SL1344 at an MOI of 10 for 4 h.
- (J) Western blot analysis and relative intensity of WT and *Nlrp6*^{-/-} MEFs treated with vehicle or MK2-IN-1 for 30 min, followed by infection with SL1344 at an MOI of 10 for 4 h. Data were compared with independent Student's *t* test. Values are expressed as the mean \pm SEM, and statistically significant differences are indicated. All data are representative of at least three independent experiments. **p* < 0.05; ***p* < 0.01; ****p* < 0.001; ns, not significant.

and *Nlrp6*^{-/-} MEFs (Figure 3F). At 4 h post-infection, a dramatically higher accumulation of phosphorylated p38^{MAPK} was detected in *Nlrp6*^{-/-} than in WT MEFs (Figure 3G). Our data further showed that pharmacological inhibition of MK2 activity reversed the significant difference in NLRP6-caused cell death, and NLRP6 suppressed MK2 phosphorylation in *S. typhimurium*-infected MEFs (Figures 3H and 3I). Importantly, there were no apparent differences in the phosphorylation of RIP1 at S321 between these two groups of infected MEFs following administration with the MK2 inhibitor (Figure 3J). These findings demonstrate a role for the TAK1-p38^{MAPK}-MK2 kinase cascade in NLRP6-associated necroptosis-dependent enterocyte injury during *S. typhimurium* infection.

NLRP6 modulates enterocyte and macrophage necroptosis during *S. typhimurium* infection

To investigate whether NLRP6-associated necroptosis occurs in IECs and macrophages, we performed *in vitro* infection experiments using Caco-2 cells and BMDMs. Our data show that diminishing the activity of MLKL, RIP3, or RIP1 resulted in the abrogation of the significant difference in cell death caused by NLRP6 (Figures 4A, 4C, S4A, and S4C). Western blot analyses show that *S. typhimurium* infection induced a significantly lower phosphorylated level of MLKL and RIP1 (S166) in NLRP6-deficient cells as compared to WT cells (Figures 4B–4D, S4B, and S4D). Importantly, *S. typhimurium* infected NLRP6-deficient cells displayed an apparent higher phosphorylated level of RIP1 at S320(human)/S321(mouse) when compared to WT cells (Figures 4E and S4E). These observations indicate that NLRP6 initiated necroptosis in both enterocytes and macrophages during *S. typhimurium* infection. We subsequently confirm the mechanism underlying the regulation of necroptosis by NLRP6. Our data showed that treatment with (5Z)-7-Oxozeaenol, SB239063, or MK2-IN-1 increased the number of dead cells in the infected NLRP6-deficient cells, which is similar to the WT cell results following inhibitor administration (Figures 4F, 4G, 4I, and S4F–S4H). Moreover, significantly higher levels of phosphorylated p38^{MAPK} and MK-2 were observed in NLRP6-deficient cells when compared to WT cells during infection (Figures 4H–4J and S4I). These observations demonstrate that NLRP6 enhances *S. typhimurium* associated necroptosis through a TAK1-p38^{MAPK}-MK2-dependent manner in both enterocytes and macrophages. Given that enterocyte cell death is one of the main reasons for the destruction of barrier function,³⁰ we further explored whether NLRP6-associated enterocyte necroptosis could influence intestinal permeability. As shown in Figure 4K, *S. typhimurium* infection resulted in a time-dependent decrease in transepithelial electrical resistance (TEER), and this decrease was greater in WT Caco-2 cell monolayers than *NLRP6*^{-/-} Caco-2 cell monolayers. Consistently, lower level of 4-kDa FITC-dextran (FD4) permeability and bacterial translocation were observed in *NLRP6*^{-/-} Caco-2 cell monolayers compared with WT Caco-2 cell monolayers after infection (Figures 4L and 4M), suggesting that NLRP6-initiated necroptosis contributed to the systemic dissemination of bacteria.

NLRP6-mediated regulation of RIP1 kinase activity contributes to *S. typhimurium*-induced necroptosis *in vivo*

To investigate whether NLRP6 worsens the outcome of Gram-negative bacterial infection and induces necroptosis *in vivo*, a well-established infection model of mouse administered with *S. typhimurium* orally was used. We found that the intestinal permeability, determining by luminal mucosa-to-blood flux of the paracellular marker FD4, and bacterial burden in MLN and systemic organs were significantly higher in WT mice than in *Nlrp6*^{-/-} mice (Figures 5A–5D). These data indicate that NLRP6 facilitates bacterial dissemination. Our *in vitro* experiments demonstrated a role for NLRP6 in promoting necroptosis in both hematopoietic (macrophages) and non-hematopoietic cells (epithelial cells). Therefore, we further generated an infection model of bone marrow chimeras. Our data show that NLRP6-deficiency in either hematopoietic and non-hematopoietic cells provided protection against *S. typhimurium* infection and spread, suggesting that NLRP6 acts as a pro-pathogen factor in both cell types (Figures 5E–5G). To determine if observed differences were due to changes in microbiome composition caused by NLRP6 deficiency, WT and *Nlrp6*^{-/-} mice were co-housed for 4 weeks and then infected with *S. typhimurium*. Similarly, the WT mice had apparent higher bacterial loads in systemic organs than the *Nlrp6*^{-/-} mice (Figures 5H–5J).

We subsequently assessed the effect of NLRP6 on necroptosis during *S. typhimurium* infection. Immunohistochemical analysis showed no significant difference in phosphorylated MLKL in the ileum between WT and *Nlrp6*^{-/-} mice (Figure S5A). However, colonic p-MLKL protein

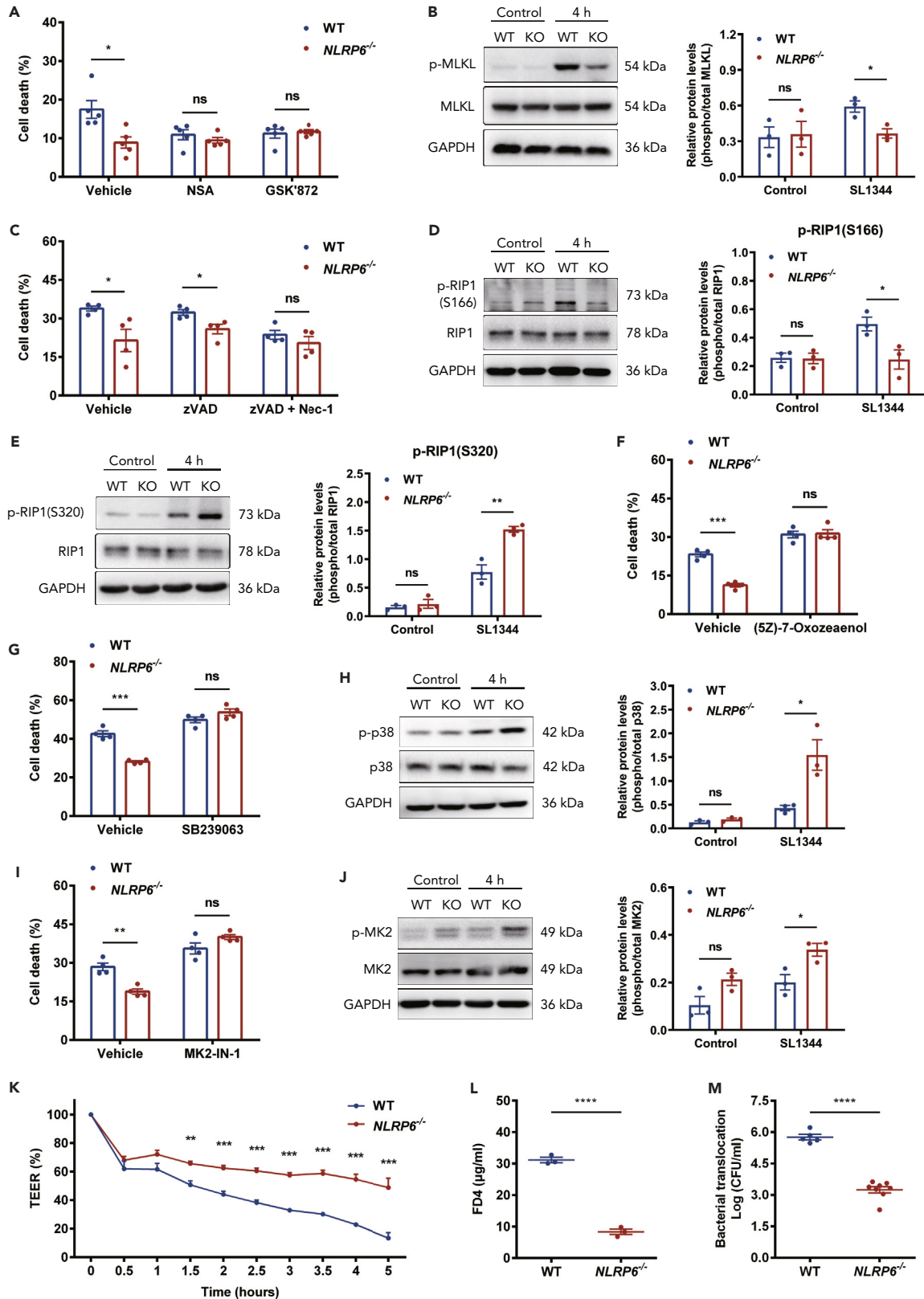


Figure 4. NLRP6 deficiency decreases *S. typhimurium*-induced enterocyte necroptosis and intestinal barrier dysfunction

- (A) Cell death of WT and *NLRP6*^{-/-} Caco-2 cells treated with vehicle, NSA or GSK'872 for 1 h, followed by infection with *S. typhimurium* strain SL1344 at an MOI of ~100 for 4 h.
- (B) Western blot analysis and relative intensity of WT and *NLRP6*^{-/-} Caco-2 cells infected with SL1344 at an MOI of ~100 for 4 h.
- (C) Cell death of WT and *NLRP6*^{-/-} Caco-2 cells treated with vehicle, zVAD or zVAD + Nec-1 for 1 h, followed by infection with *S. typhimurium* strain SL1344 at an MOI of ~100 for 4 h.
- (D and E) Western blot analysis and relative intensity of WT and *NLRP6*^{-/-} Caco-2 cells infected with SL1344 at an MOI of ~100 for 4 h.
- (F) Cell death of WT and *NLRP6*^{-/-} Caco-2 cells treated with vehicle or (5Z)-7-Oxozeaenol for 1 h, followed by infection with SL1344 at an MOI of ~100 for 4 h.
- (G) Cell death of WT and *NLRP6*^{-/-} Caco-2 cells treated with vehicle or SB239063 for 30 min, followed by infection with SL1344 at an MOI of ~100 for 4 h.
- (H) Western blot analysis and relative intensity of WT and *NLRP6*^{-/-} Caco-2 cells infected with SL1344 at an MOI of ~100 for 4 h.
- (I) Cell death of WT and *NLRP6*^{-/-} Caco-2 cells treated with vehicle or MK2-IN-1 for 30 min, followed by infection with SL1344 at an MOI of ~100 for 4 h.
- (J) Western blot analysis and relative intensity of WT and *NLRP6*^{-/-} Caco-2 cells infected with SL1344 at an MOI of ~100 for 4 h.
- (K) TEER levels of WT and *NLRP6*^{-/-} Caco-2 cell monolayers infected with SL1344 at an MOI of ~100.
- (L) FD4 permeability of WT and *NLRP6*^{-/-} Caco-2 cell monolayers infected with SL1344 at an MOI of ~100 for 3 h.
- (M) Bacterial translocation of WT and *NLRP6*^{-/-} Caco-2 cell monolayers infected with SL1344 at an MOI of ~100 for 3 h. Data were compared with independent Student's *t* test. Values are expressed as the mean ± SEM, and statistically significant differences are indicated. All data are representative of at least three independent experiments. **p* < 0.05; ***p* < 0.01; ****p* < 0.001; *****p* < 0.0001; ns, not significant.

levels were significantly lower in *S. typhimurium*-infected *Nlrp6*^{-/-} mice than in wild-type mice (Figure 5K). To test whether this phenotype was present in enterocytes, either ileal or colonic IECs were isolated from WT and *Nlrp6*^{-/-} mice with or without infection. In line with data obtained in the immunohistochemical stain assay, similar phosphorylated levels of MLKL, RIP1(S321), and RIP1(S166) were observed in the ileum of WT and *Nlrp6*^{-/-} mice, whereas the infected *Nlrp6*^{-/-} mice had a significantly lower level of MLKL phosphorylation in the colon as compared with those in infected WT mice (Figures S5B, 5L, and 5M). Meanwhile, NLRP6 deficiency resulted in an increased phosphorylated RIP1 at S321 and a decreased phosphorylated RIP1 at S166 in colonic IECs (Figures 5L and 5M), suggesting that NLRP6 facilitated necroptosis in the colon through regulating the kinase activity of RIP1. In addition, although a higher level of p-RIP1(S321) was found in the spleen of *Nlrp6*^{-/-} mice compared with those of WT mice, no significant difference was observed between the expression of p-MLKL and p-RIP1(S166) of these two genotypes during infection (Figures S6A and S6B). To confirm the role of RIP1 in NLRP6-associated intestinal bacteria dissemination and colonic necroptosis, *S. typhimurium*-infected mice were administrated with the RIP1 inhibitor Nec-1s. Our data showed that the significant difference in intestinal permeability, tissue bacterial burden and colonic necroptosis between the wild-type and the *Nlrp6*^{-/-} mice was abrogated by Nec-1s (Figures 6A–6F). To better understand the observed mechanisms underlying NLRP6-relevant necroptosis, p38^{MAPK} and MK2 phosphorylation in colonic IECs were quantified. Consistent with our *in vitro* observations, *S. typhimurium* infection led to an increase of both p38^{MAPK} and MK2 phosphorylation, and p-p38^{MAPK} and p-MK2 protein levels were significantly higher in infected *Nlrp6*^{-/-} than in WT mice (Figure 6G). Treatment of *S. typhimurium*-infected mice with the MK2 inhibitor abolished the significant difference in necroptosis between WT and *Nlrp6*^{-/-} colonic IECs (Figures 6I and 6J). Importantly, the significant difference in tissue bacterial burden between the wild-type and the *Nlrp6*^{-/-} mice was also reversed by PF-3644022 (Figures 6K–6M). Taken together, these *in vivo* data further support our results obtained *in vitro*, showing that NLRP6 modulates RIP1-mediated MLKL phosphorylation and necroptosis during *S. typhimurium* infection.

DISCUSSION

In the current study, we aimed to elucidate the underlying interconnection between NLRP6 and cell death during Gram-negative bacterial infection. Using well-established models of *S. typhimurium* infection both *in vitro* and *in vivo*, we provide what is, to our knowledge, the first report that NLRP6 has a detrimental effect on host antimicrobial response through modulating the initiation of necroptosis. Our data uncovered a novel mechanism underlying NLRP6-mediated necroptosis during *S. typhimurium* infection. This process is orchestrated via activation of RIP1 kinase-dependent MLKL, which resulted from a decrease in RIP1 phosphorylation at S321 induced by TAK1-mediated p38^{MAPK}/MK2 phosphorylation. Therefore, NLRP6 may be utilized by *S. typhimurium* to disrupt the intestinal barrier and for subsequent systemic dissemination.

Emerging evidence demonstrates that NLRP6 plays a multifaceted role in pathogenic organism infection. By binding with the RNA helicase DEAH (Asp-Glu-Ala-His) box helicase 15 (Dhx15), NLRP6 detects viruses and initiates type I interferon (IFN) responses in an inflammasome-independent manner.³¹ However, NLRP6 could also protect hosts against RNA virus and the intestinal parasite *Cryptosporidium* in an inflammasome-dependent manner.^{32,33} Similar responses have been described in Gram-positive bacterial infection. By recognizing Lipoteichoic acid, a product of Gram-positive bacteria, NLRP6 formed an inflammasome component and activated macrophage function that restricts *Staphylococcus aureus*-induced pneumonia.⁸ To explore the role of NLRP6 in host defense Gram-negative bacterial infection, our present study established a well-known model of *S. typhimurium* infection and reported that NLRP6 is associated with cell death both in hematopoietic cells (macrophages) and non-hematopoietic cells (IECs and MEFs). A dramatically increased number of dead cells, along with a significantly decreased number of viable cells, was observed in WT cells, whereas NLRP6-deficient cells were highly resistant to *S. typhimurium*-induced cell death.

Pyroptosis is type of PCD occurring in a wide range of microbial infections.³⁴ Previous research from other laboratories has reported that several members of the NLR family can trigger an inflammasome-associated downstream signaling cascade that initiates pyroptosis and forms GSDMD-mediated membrane pores.³⁵ A recent study reported that NLRP6 deficiency also led to a decrease of pyroptosis during

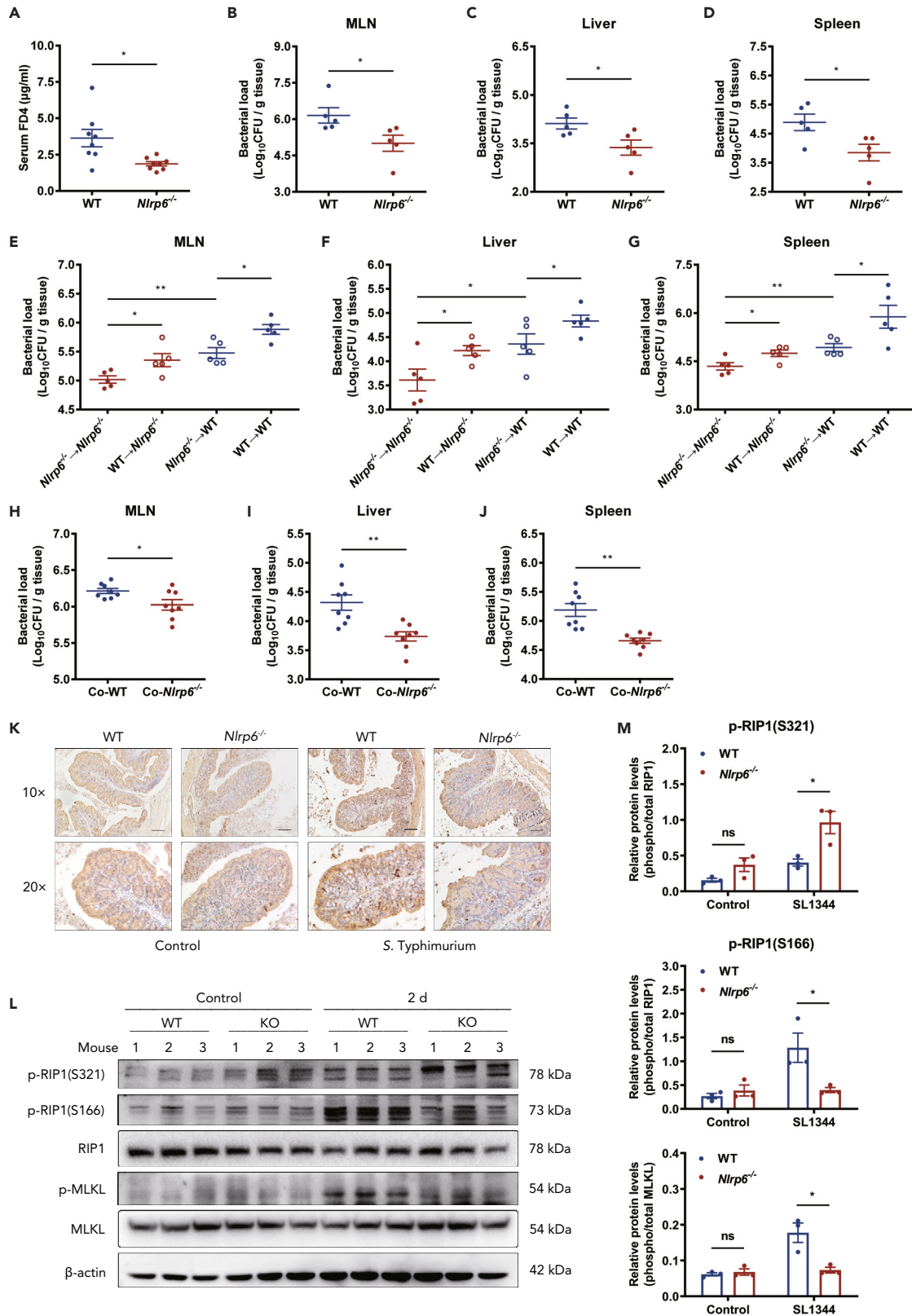


Figure 5. NLRP6 promotes *S. typhimurium*-induced intestinal barrier dysfunction and necroptosis in vivo

(A–D) Streptomycin-pretreated WT and *Nlrp6*^{-/-} mice were orally infected with 5×10^7 CFU of *S. typhimurium* strain SL1344 and analyzed at 3 days post-infection. Intestinal permeability (A). Bacterial burden in MLN (B), liver (C) and spleen (D).

(E–G) Streptomycin-pretreated bone marrow chimeras were orally infected with 5×10^7 CFU of SL1344 and analyzed at 3 days post-infection. Bacterial burden in MLN (E), liver (F) and spleen (G).

(H–J) WT and *Nlrp6*^{-/-} mice were co-housed together for 4 weeks, and then orally infected with 5×10^7 CFU of SL1344 and analyzed at 3 days post-infection. Bacterial burden in MLN (H), liver (I) and spleen (J).

(K–M) Streptomycin-pretreated WT and *Nlrp6*^{-/-} mice were orally infected with 1×10^8 CFU of *S. typhimurium* strain SL1344 and analyzed at 2 days post-infection. Immunohistochemical staining of colon sections. scale bars: 100 μ m (K). Western blot analysis and relative intensity of colonic intestinal epithelial cells isolated from mice (L, M). Data were compared with independent Student's *t* test. Values are expressed as the mean \pm SEM, and statistically significant differences are indicated. All data are representative of at least three independent experiments. **p* < 0.05; ***p* < 0.01; ns, not significant.

Gram-positive bacterial infection.¹⁰ Interestingly, our data show that NLRP6 had little effect on *S. typhimurium*-induced cleavage of GSDMD. Blocking GSDMD processing could not reverse the significant difference in NLRP6-induced cell death. These results indicate that NLRP6 mediated cell death via a pyroptosis-independent pathway. Therefore, we will focus our next study on necroptosis, another common type of lytic PCD that is triggered following challenge with several pathogens.

Necroptosis is induced by MLKL-mediated formation of necroptotic pores and manifests as plasma membrane rupture. It has been demonstrated that the MLKL inhibitor NSA interferes with disulfide bond formation of MLKL in humans but not in murine MLKL.³⁶ Hence, we treated human Caco-2 and HeLa cells with NSA and administered murine MEFs and BMDMs with another MLKL inhibitor GW806742X. Our data show that suppression of MLKL significantly decreased NLRP6-mediated cell death among macrophages, IECs, and MEFs. The following data further support NLRP6 functions in amplifying necroptosis in *S. typhimurium*-infected cells: (1) Knockdown of NLRP6 resulted in decreased phosphorylated levels of MLKL; (2) a higher percentage of dead cells was observed in HeLa cells co-expressing RIP3 and NLRP6; and (3) downregulation of RIP1 activity reversed the apparent difference in cell death caused by NLRP6. Laxman Ghimire et al. recently reported that NLRP6-mediated necroptosis occurred during Gram-positive bacterial infection; however, the underlying mechanism has not yet been reported.¹⁰ In the present study, our observations expand the understanding of NLRP6 also triggering necroptosis during Gram-negative bacterial infection through a RIP1 kinase-dependent mechanism, and further demonstrated that the RIP1 inhibitor could effectively alleviate NLRP6-induced intestinal barrier dysregulation and the spread of enteropathogenic bacteria.

It has been reported that RIP1 kinase activity could be prevented via the NF- κ B signaling pathway.³⁷ Anand et al. reported that NLRP6 alone was capable of inhibiting NF- κ B activity, leading to the reduction of the inflammatory response and bacterial clearance in hematopoietic cells (macrophages and neutrophils).⁹ Our data show that NLRP6 also contributed to the downregulation of I κ B α degradation in non-hematopoietic cells and suppressed IL1 β , TNF α , or PMA-induced NF- κ B activation. We subsequently investigated component functions as a potential NLRP6 target and observed that NLRP6 downregulated NF- κ B activity in TRAF6 or TRAF2 overexpressed cells but not in TAK1/TAB1, IKK β , or p65 overexpressed cells. These results suggest that NLRP6 regulated NF- κ B activation by targeting the components of TAK1. Our results further showed that NLRP6 inhibits necroptosis through downregulating the phosphorylation of TAK1 rather than protein stability. Previous studies demonstrated that the p38^{MAPK}/MK2 module, a signaling cascade downstream of TAK1, has an essential role in controlling necroptosis, and MK2 is the unique molecular that directly phosphorylates RIP1 at S321, a residue that suppresses RIP1 S166 auto-phosphorylation.³⁸ Our data show that NLRP6 deficiency resulted in an apparent increased phosphorylation of p38^{MAPK}, MK2 and RIP1 S321 both *in vitro* and *in vivo*. Importantly, downregulation of either p38^{MAPK} or MK2 not only blocked the inhibitory effect of NLRP6 on RIP1(S321) phosphorylation but also abrogated the apparent difference in NLRP6-relevant cell death during infection.

In summary, our data report a novel detrimental role for NLRP6 in promoting RIP1 kinase-dependent necroptosis, but not pyroptosis, during *S. typhimurium* infection. We found that NLRP6 *per se* inhibits NF- κ B pathway activity by downregulating TAK1 phosphorylation and subsequently contributes to a reduction in p38^{MAPK}/MK2 signaling cascade downstream of TAK1. Decreased MK2 phosphorylation resulted in a decrease in its phosphorylated target residue on S321 of RIP1, thus ultimately increasing RIP1-kinase-dependent phosphorylation and activation of the necroptosis executor MLKL. Therapeutic strategies targeting NLRP6 might be advantageous for decreasing Gram-negative bacteria-induced cell death and thus controlling infection.

Limitations of the study

This study uncovered the role of NLRP6 in regulating necroptotic cell death during *S. typhimurium* infection. Although our observations suggest NLRP6 as a therapeutic target for decreasing bacteria-induced host cell death and controlling the spread of *S. typhimurium*, it remains to be seen if NLRP6 is also required for orchestrating necroptosis induced by other enteropathogenic bacterial. In addition, it is worth figuring out how NLRP6 interacts with TAK1 and selectively modulates its ubiquitination modification in future.

STAR★METHODS

Detailed methods are provided in the online version of this paper and include the following:

- KEY RESOURCES TABLE

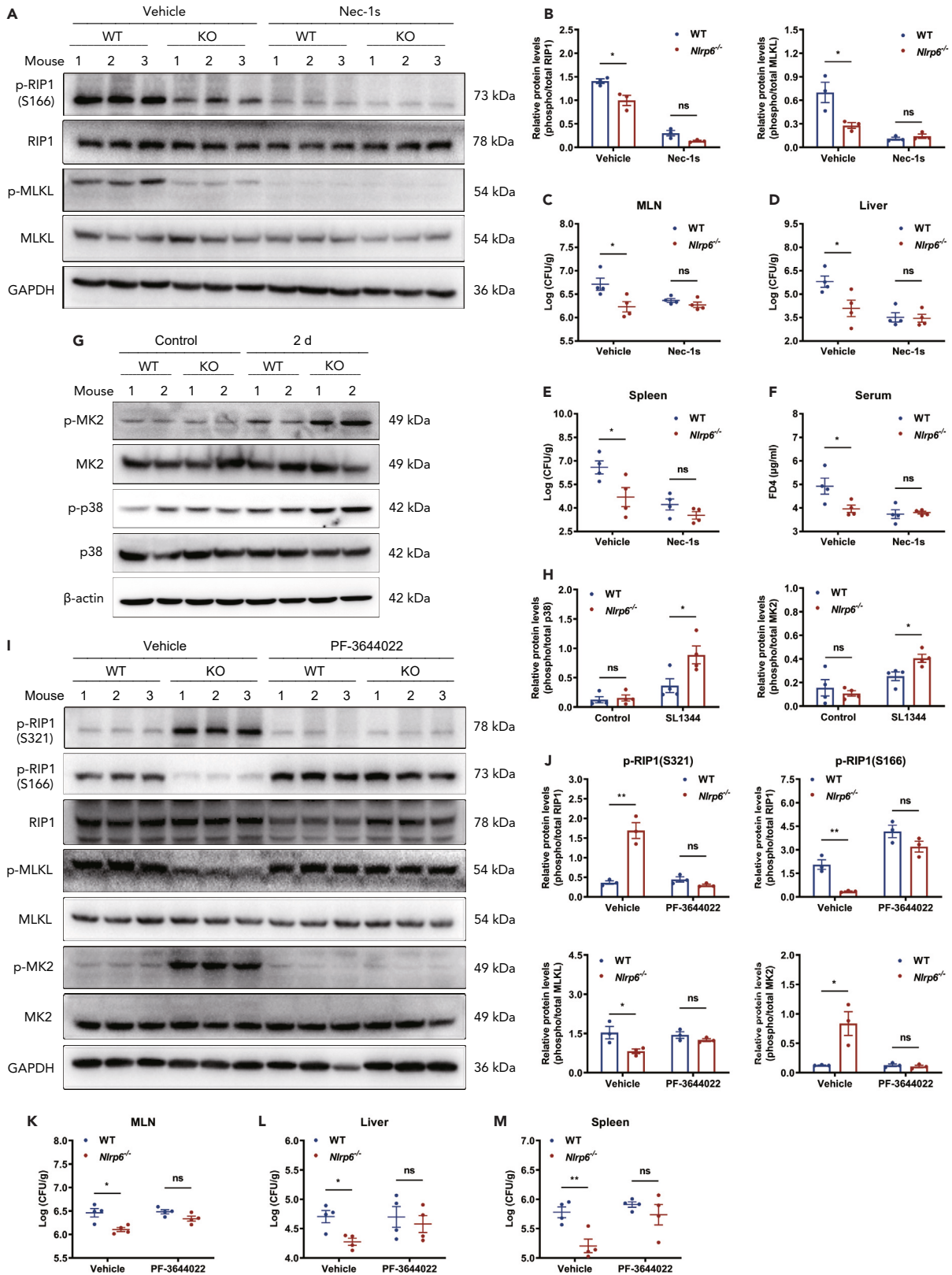


Figure 6. NLRP6 promotes the systemic dissemination of *S. typhimurium* by regulating MK2/RIP1-associated necroptosis *in vivo*

(A–F) Streptomycin-pretreated WT and *Nlrp6*^{−/−} mice were orally infected with 1×10^8 CFU of *S. typhimurium* strain SL1344. Mice were administrated intraperitoneally with the RIP1 inhibitor Nec-1s at 1 h prior to infection and 24 h post-infection, followed by sample collection at 2 days post-infection. Western blot analysis and relative intensity of colonic intestinal epithelial cells isolated from mice (A, B). Bacterial burden in MLN (C), liver (D) and spleen (E). Intestinal permeability (F).

(G and H) Streptomycin-pretreated WT and *Nlrp6*^{−/−} mice were orally infected with 1×10^8 CFU of SL1344 and analyzed at 2 days post-infection. Western blot analysis and relative intensity of colonic intestinal epithelial cells isolated from mice.

(I–M) Streptomycin-pretreated WT and *Nlrp6*^{−/−} mice were orally infected with 1×10^8 CFU of SL1344 and administrated orally with the MK2 inhibitor PF-3644022 at 4 h post-infection, followed by sample collection at 2 days post-infection. Western blot analysis and relative intensity of colonic intestinal epithelial cells isolated from mice (I, J). Bacterial burden in MLN (K), liver (L) and spleen (M). Data were compared with independent Student's *t* test. Values are expressed as the mean \pm SEM, and statistically significant differences are indicated. **p* < 0.05; ***p* < 0.01; ****p* < 0.001; ns, not significant.

● RESOURCE AVAILABILITY

- Lead contact
- Materials availability
- Data and code availability

● EXPERIMENTAL MODEL AND STUDY PARTICIPANT DETAILS

- Animals
- Cell culture studies
- Bacterial strains

● METHOD DETAILS

- Cell preparation
- Bacteria preparation
- *S. Typhimurium* infection *in vitro*
- Plasmid, siRNA and Transfection experiments
- Cell death and viability assays
- Western blot analysis
- Protein stability assay
- Immunoprecipitation and ubiquitination assay
- TEER and epithelial permeability assay
- Caspase substrate cleavage assay
- ELISA
- Luciferase reporter assays
- Mouse experiments and ethics statement

● QUANTIFICATION AND STATISTICAL ANALYSIS**SUPPLEMENTAL INFORMATION**

Supplemental information can be found online at <https://doi.org/10.1016/j.isci.2024.109339>.

ACKNOWLEDGMENTS

The authors thank Professor Ying Xu (Cambridge-Suda Genome Resource Center, Soochow University, Suzhou, China) for providing excellent technical assistance and her insightful suggestions, Associate Professor Jing Xu (School of Biology & Basic Medical Sciences, Soochow University, Suzhou, China) for assistance in creation of bone marrow chimeric mice, Ying Ye (Cambridge-Suda Genome Resource Center, Soochow University, Suzhou, China) for assistance in isolation of mouse embryonic fibroblasts. The work is supported by National Natural Science Foundation of China (81971899, 31970132, 82202534, 32200109), China Postdoctoral Science Foundation (BX20220358, 2022M710172, 2022T150750), Guangdong Basic and Applied Basic Research Foundation (2021A1515110198) and a project funded by the Priority Academic Program Development (PAPD) of Jiangsu Higher Education Institutions.

AUTHOR CONTRIBUTIONS

Conceptualization, Q.D., S.Y., and R.H.; Methodology, Q.D., S.Y., and K.H.; Formal Analysis, Q.D., S.Y., and K.H.; Investigation, Q.D., S.Y., K.H., Y.Z., L.S., Y.C., K.D., and Y.L.; Resources, R.H.; Writing – Original Draft, Q.D., S.Y., and R.H.; Writing – Review and Editing, Y.L., S.W., and R.H.; Supervision, R.H.; Funding Acquisition, R.H., S.W., Q.D., and S.Y.

DECLARATION OF INTERESTS

The authors declare no conflicts of interest.

Received: April 23, 2023

Revised: November 16, 2023

Accepted: February 22, 2024

Published: February 28, 2024

REFERENCES

- Degterev, A., Huang, Z., Boyce, M., Li, Y., Jagtap, P., Mizushima, N., Cuny, G.D., Mitchison, T.J., Moskowitz, M.A., and Yuan, J. (2005). Chemical inhibitor of nonapoptotic cell death with therapeutic potential for ischemic brain injury. *Nat. Chem. Biol.* 1, 112–119. <https://doi.org/10.1038/nchembio711>.
- Xia, X., Lei, L., Wang, S., Hu, J., and Zhang, G. (2020). Necroptosis and its role in infectious diseases. *Apoptosis* 25, 169–178. <https://doi.org/10.1007/s10495-019-01589-x>.
- Mompeán, M., Li, W., Li, J., Laage, S., Siemer, A.B., Bozkurt, G., Wu, H., and McDermott, A.E. (2018). The Structure of the Necrosome RIPK1-RIPK3 Core, a Human Hetero-Amyloid Signaling Complex. *Cell* 173, 1244–1253.e10. <https://doi.org/10.1016/j.cell.2018.03.032>.
- Pasparakis, M., and Vandenabeele, P. (2015). Necroptosis and its role in inflammation. *Nature* 517, 311–320. <https://doi.org/10.1038/nature14191>.
- Frank, D., and Vince, J.E. (2019). Pyroptosis versus necroptosis: similarities, differences, and crosstalk. *Cell Death Differ.* 26, 99–114. <https://doi.org/10.1038/s41418-018-0212-6>.
- Levy, M., Shapiro, H., Thaisz, C.A., and Elinav, E. (2017). NLRP6: A Multifaceted Innate Immune Sensor. *Trends Immunol.* 38, 248–260. <https://doi.org/10.1016/j.it.2017.01.001>.
- Ghimire, L., Paudel, S., Jin, L., and Jeyaseelan, S. (2020). The NLRP6 inflammasome in health and disease. *Mucosal Immunol.* 13, 388–398. <https://doi.org/10.1038/s41385-020-0256-z>.
- Hara, H., Seregin, S.S., Yang, D., Fukase, K., Chamailard, M., Alnemri, E.S., Inohara, N., Chen, G.Y., and Núñez, G. (2018). The NLRP6 Inflammasome Recognizes Lipoteichoic Acid and Regulates Gram-Positive Pathogen Infection. *Cell* 175, 1651–1664.e14. <https://doi.org/10.1016/j.cell.2018.09.047>.
- Anand, P.K., Malireddi, R.K.S., Lukens, J.R., Vogel, P., Bertin, J., Lamkanfi, M., and Kanneganti, T.D. (2012). NLRP6 negatively regulates innate immunity and host defence against bacterial pathogens. *Nature* 488, 389–393. <https://doi.org/10.1038/nature11250>.
- Ghimire, L., Paudel, S., Jin, L., Baral, P., Cai, S., and Jeyaseelan, S. (2018). NLRP6 negatively regulates pulmonary host defense in Gram-positive bacterial infection through modulating neutrophil recruitment and function. *PLoS Pathog.* 14, e1007308. <https://doi.org/10.1371/journal.ppat.1007308>.
- Garai, P., Gnanadhas, D.P., and Chakravorty, D. (2012). Salmonella enterica serovars Typhimurium and Typhi as model organisms: revealing paradigm of host-pathogen interactions. *Virulence* 3, 377–388. <https://doi.org/10.4161/viru.21087>.
- Wotzka, S.Y., Nguyen, B.D., and Hardt, W.D. (2017). Salmonella Typhimurium Diarrhea Reveals Basic Principles of Enteropathogen Infection and Disease-Promoted DNA Exchange. *Cell host & microbe* 21, 443–454. <https://doi.org/10.1016/j.chom.2017.03.009>.
- Wemyss, M.A., and Pearson, J.S. (2019). Host Cell Death Responses to Non-typhoidal Salmonella Infection. *Front. Immunol.* 10, 1758. <https://doi.org/10.3389/fimmu.2019.01758>.
- Sellin, M.E., Müller, A.A., Felmy, B., Dolowschiak, T., Diard, M., Tardivel, A., Maslowski, K.M., and Hardt, W.D. (2014). Epithelium-intrinsic NAIIP/NLRC4 inflammasome drives infected enterocyte expulsion to restrict Salmonella replication in the intestinal mucosa. *Cell host & microbe* 16, 237–248. <https://doi.org/10.1016/j.chom.2014.07.001>.
- Ashida, H., Mimuro, H., Ogawa, M., Kobayashi, T., Sanada, T., Kim, M., and Sasakawa, C. (2011). Cell death and infection: a double-edged sword for host and pathogen survival. *J. Cell Biol.* 195, 931–942. <https://doi.org/10.1083/jcb.201108081>.
- Robinson, N., McComb, S., Mulligan, R., Dudani, R., Krishnan, L., and Sad, S. (2012). Type I interferon induces necroptosis in macrophages during infection with Salmonella enterica serovar Typhimurium. *Nat. Immunol.* 13, 954–962. <https://doi.org/10.1038/ni.2397>.
- Hos, N.J., Ganesan, R., Gutiérrez, S., Hos, D., Klimek, J., Abdullah, Z., Krönke, M., and Robinson, N. (2017). Type I interferon enhances necroptosis of Salmonella Typhimurium-infected macrophages by impairing antioxidant stress responses. *J. Cell Biol.* 216, 4107–4121. <https://doi.org/10.1083/jcb.201701107>.
- Hefele, M., Stolzer, I., Ruder, B., He, G.W., Mahapatro, M., Wirtz, S., Neurath, M.F., and Günther, C. (2018). Intestinal epithelial Caspase-8 signaling is essential to prevent necroptosis during Salmonella Typhimurium induced enteritis. *Mucosal Immunol.* 11, 1191–1202. <https://doi.org/10.1038/s41385-018-0011-x>.
- Deng, Q., Yang, S., Sun, L., Huang, K., Dong, K., Zhu, Y., Cao, Y., Li, Y., Wu, S., and Huang, R. (2022). A detrimental role of NLRP6 in host iron metabolism during Salmonella infection. *Redox Biol.* 49, 102217. <https://doi.org/10.1016/j.redox.2021.102217>.
- Mastroeni, P., Grant, A., Restif, O., and Maskell, D. (2009). A dynamic view of the spread and intracellular distribution of Salmonella enterica. *Nat. Rev. Microbiol.* 7, 73–80. <https://doi.org/10.1038/nrmicro2034>.
- Zhang, Y., Chen, X., Gueydan, C., and Han, J. (2018). Plasma membrane changes during programmed cell deaths. *Cell Res.* 28, 9–21. <https://doi.org/10.1038/cr.2017.133>.
- Degterev, A., Hitomi, J., Germscheid, M., Ch'en, I.L., Korkina, O., Teng, X., Abbott, D., Cuny, G.D., Yuan, C., Wagner, G., et al. (2008). Identification of RIP1 kinase as a specific cellular target of necrostatins. *Nat. Chem. Biol.* 4, 313–321. <https://doi.org/10.1038/nchembio.83>.
- Dhuriya, Y.K., and Sharma, D. (2018). Necroptosis: a regulated inflammatory mode of cell death. *J. Neuroinflammation* 15, 199. <https://doi.org/10.1186/s12974-018-1235-0>.
- Sai, K., Parsons, C., House, J.S., Kathariou, S., and Ninomiya-Tsuji, J. (2019). Necroptosis mediators RIPK3 and MLKL suppress intracellular Listeria replication independently of host cell killing. *J. Cell Biol.* 218, 1994–2005. <https://doi.org/10.1083/jcb.201810014>.
- Lim, J., Park, H., Heisler, J., Maculins, T., Roose-Girma, M., Xu, M., McKenzie, B., van Lookeren Campagne, M., Newton, K., and Murthy, A. (2019). Autophagy regulates inflammatory programmed cell death via turnover of RHIM-domain proteins. *Elife* 8. <https://doi.org/10.7554/eLife.44452>.
- Ashida, H., Nakano, H., and Sasakawa, C. (2013). Shigella IpaH0722 E3 ubiquitin ligase effector targets TRAF2 to inhibit PKC-NF-kappaB activity in invaded epithelial cells. *PLoS Pathog.* 9, e1003409. <https://doi.org/10.1371/journal.ppat.1003409>.
- Wang, C., Deng, L., Hong, M., Akkaraju, G.R., Inoue, J., and Chen, Z.J. (2001). TAK1 is a ubiquitin-dependent kinase of MKK and IKK. *Nature* 412, 346–351. <https://doi.org/10.1038/35085597>.
- Yan, F.J., Zhang, X.J., Wang, W.X., Ji, Y.X., Wang, P.X., Yang, Y., Gong, J., Shen, L.J., Zhu, X.Y., Huang, Z., and Li, H. (2017). The E3 ligase tripartite motif 8 targets TAK1 to promote insulin resistance and steatohepatitis. *Hepatology* 65, 1492–1511. <https://doi.org/10.1002/hep.28971>.
- Jaco, I., Annibaldi, A., Lalaoui, N., Wilson, R., Tenev, T., Laurien, L., Kim, C., Jamal, K., Wicky John, S., Liccardi, G., et al. (2017). MK2 Phosphorylates RIPK1 to Prevent TNF-Induced Cell Death. *Mol. Cell* 66, 698–710.e5. <https://doi.org/10.1016/j.molcel.2017.05.003>.
- Günther, C., Neumann, H., Neurath, M.F., and Becker, C. (2013). Apoptosis, necrosis and necroptosis: cell death regulation in the intestinal epithelium. *Gut* 62, 1062–1071. <https://doi.org/10.1136/gutjnl-2011-301364>.
- Wang, P., Zhu, S., Yang, L., Cui, S., Pan, W., Jackson, R., Zheng, Y., Rongvaux, A., Sun, Q., Yang, G., et al. (2015). Nlrp6 regulates intestinal antiviral innate immunity. *Science* 350, 826–830. <https://doi.org/10.1126/science.aab3145>.
- Sateriale, A., Gullicksrud, J.A., Engiles, J.B., McLeod, B.I., Kugler, E.M., Henao-Mejia, J., Zhou, T., Ring, A.M., Brodsky, I.E., Hunter, C.A., and Striepen, B. (2021). The intestinal parasite Cryptosporidium is controlled by an enterocyte intrinsic inflammasome that depends on NLRP6. In Proceedings of the National Academy of Sciences of the United States of America. 118. <https://doi.org/10.1073/pnas.2007807118>.
- Shen, C., Li, R., Negro, R., Cheng, J., Vora, S.M., Fu, T.M., Wang, A., He, K., Andreeva, L., Gao, P., et al. (2021). Phase separation drives RNA virus-induced activation of the NLRP6 inflammasome. *Cell* 184, 5759–5774.e20. <https://doi.org/10.1016/j.cell.2021.09.032>.
- Bedoui, S., Herold, M.J., and Strasser, A. (2020). Emerging connectivity of programmed cell death pathways and its

- physiological implications. *Nat. Rev. Mol. Cell Biol.* 21, 678–695. <https://doi.org/10.1038/s41580-020-0270-8>.
35. Broz, P., Pelegrín, P., and Shao, F. (2020). The gasdermins, a protein family executing cell death and inflammation. *Nat. Rev. Immunol.* 20, 143–157. <https://doi.org/10.1038/s41577-019-0228-2>.
 36. Sun, L., Wang, H., Wang, Z., He, S., Chen, S., Liao, D., Wang, L., Yan, J., Liu, W., Lei, X., and Wang, X. (2012). Mixed lineage kinase domain-like protein mediates necrosis signaling downstream of RIP3 kinase. *Cell* 148, 213–227. <https://doi.org/10.1016/j.cell.2011.11.031>.
 37. Dondelinger, Y., Jouan-Lanhuet, S., Divert, T., Theatre, E., Bertin, J., Gough, P.J., Giansanti, P., Heck, A.J.R., Dejardin, E., Vandenabeele, P., and Bertrand, M.J.M. (2015). NF-kappaB-Independent Role of IKKalpha/IKKbeta in Preventing RIPK1 Kinase-Dependent Apoptotic and Necroptotic Cell Death during TNF Signaling. *Mol. Cell* 60, 63–76. <https://doi.org/10.1016/j.molcel.2015.07.032>.
 38. Menon, M.B., Gropengießer, J., Fischer, J., Novikova, L., Deuretzbacher, A., Lafera, J., Schimmeck, H., Czymmeck, N., Ronkina, N., Kotlyarov, A., et al. (2017). p38(MAPK)/MK2-dependent phosphorylation controls cytotoxic RIPK1 signalling in inflammation and infection. *Nat. Cell Biol.* 19, 1248–1259. <https://doi.org/10.1038/ncb3614>.
 39. Yang, S., Deng, Q., Sun, L., Dong, K., Li, Y., Wu, S., and Huang, R. (2019). Salmonella effector SpvB interferes with intracellular iron homeostasis via regulation of transcription factor NRF2. *FASEB. J.* 33, 13450–13464. <https://doi.org/10.1096/fj.201900883RR>.
 40. Tang, Y., Tu, H., Zhang, J., Zhao, X., Wang, Y., Qin, J., and Lin, X. (2019). K63-linked ubiquitination regulates RIPK1 kinase activity to prevent cell death during embryogenesis and inflammation. *Nat. Commun.* 10, 4157. <https://doi.org/10.1038/s41467-019-12033-8>.
 41. Burkholder, K.M., and Bhunia, A.K. (2010). *Listeria monocytogenes* uses *Listeria* adhesion protein (LAP) to promote bacterial transepithelial translocation and induces expression of LAP receptor Hsp60. *Infect. Immun.* 78, 5062–5073. <https://doi.org/10.1128/IAI.00516-10>.
 42. Yang, S., Deng, Q., Sun, L., Zhu, Y., Dong, K., Wu, S., Huang, R., and Li, Y. (2021). Salmonella Effector SpvB Inhibits NF-kappaB Activity via KEAP1-Mediated Downregulation of IKKbeta. *Front. Cell. Infect. Microbiol.* 11, 641412. <https://doi.org/10.3389/fcimb.2021.641412>.
 43. Deng, Q., Yang, S., Sun, L., Dong, K., Li, Y., Wu, S., and Huang, R. (2021). Salmonella effector SpvB aggravates dysregulation of systemic iron metabolism via modulating the hepcidin-ferroportin axis. *Gut Microb.* 13, 1–18. <https://doi.org/10.1080/19490976.2020.1849996>.
 44. Nenci, A., Becker, C., Wullaert, A., Gareus, R., van Loo, G., Danese, S., Huth, M., Nikolaev, A., Neufert, C., Madison, B., et al. (2007). Epithelial NEMO links innate immunity to chronic intestinal inflammation. *Nature* 446, 557–561. <https://doi.org/10.1038/nature05698>.

STAR★METHODS

KEY RESOURCES TABLE

REAGENT or RESOURCE	SOURCE	IDENTIFIER
Antibodies		
Anti-mouse GSDMD	Abcam	Cat# ab219800; RRID: AB_2888940
Anti-human GSDMD	Abcam	Cat# ab210070; RRID: AB_2893325
Anti-mouse phospho-MLKL	Abcam	Cat# ab196436; RRID: AB_2687465
Anti-human phospho-MLKL	Abcam	Cat# ab187091; RRID: AB_2619685
Anti-MLKL	Proteintech	Cat# 66675-1-Ig; RRID: AB_2882029
Anti-mouse phospho-RIP1(Ser166)	Affinity	Cat# AF2398; RRID: AB_2845412
Anti-human phospho-RIP1(Ser166)	Immunoway	Cat# YP1467; RRID: AB_3094761
Anti-mouse phospho-RIP1(Ser321)	Cell Signaling Technology	Cat# 38662; RRID: AB_3094762
Anti-human phospho-RIP1(Ser320)	Cell Signaling Technology	Cat# 58274; RRID: AB_2933988
Anti-RIP1	Cell Signaling Technology	Cat# 3493; RRID: AB_2305314
Anti-IkB α	Proteintech	Cat# 10268-1-AP; RRID: AB_2151423
Anti-phospho-TAK1	Cell Signaling Technology	Cat# 4536; RRID: AB_330493
Anti-TAK1	Proteintech	Cat# 12330-2-AP; RRID: AB_2140101
Anti-phospho-p38MAPK	Cell Signaling Technology	Cat# 4511; RRID: AB_2139682
Anti-p38MAPK	Cell Signaling Technology	Cat# 9212; RRID: AB_330713
Anti-phospho-MK2	Cell Signaling Technology	Cat# 3007; RRID: AB_490936
Anti-MK2	Proteintech	Cat# 13949-1-AP; RRID: AB_2877995
Anti-Ubiquitin	Cell Signaling Technology	Cat# 43124; RRID: AB_2799235
Anti-Horseradish peroxidase (HRP) Flag	Sigma-Aldrich	Cat# A8592; RRID: AB_439702
Anti-6 \times His	Thermo Fisher Scientific	Cat# MA1-21315; RRID: AB_557403
Anti- β -actin	Bioss	Cat# bs-0061R; RRID: AB_10855480
Anti-GAPDH	Boster	Cat# BM1623; RRID: AB_2885058
Anti- α -Tubulin	Beyotime Biotechnology	Cat# AF0001; RRID: AB_2922414
Bacterial and virus strains		
<i>S. Typhimurium</i> strain SL1344	Yang et al. ³⁹	N/A
Chemicals, peptides, and recombinant proteins		
RPMI 1640 medium	HyClone Laboratories	Cat# SH30096.01
Fetal bovine serum (FBS)	Biological Industries	Cat# 04-121-1A
Macrophage Colony Stimulating Factor (M-CSF)	PepruTech	Cat# 315-02
1% (vol/vol) penicillin-streptomycin	Beyotime Biotechnology	Cat# C0222
Dulbecco's Modified Eagle Medium (DMEM)	HyClone Laboratories	Cat# SH30243.01
PBS	Sangon Biotech	Cat# E607008
Gentamicin	Sangon Biotech	Cat# A506614
GW806742X	MCE	Cat# HY-112292
NSA	MCE	Cat# HY-100573
GSK'872	MCE	Cat# HY-101872
zVAD	Beyotime Biotechnology	Cat# C1202
Nec-1	MCE	Cat# HY-15760
(5Z)-7-Oxozeaenol	Ape \times Bio	Cat# b7443
SB239063	MCE	Cat# HY-11068

(Continued on next page)

Continued

REAGENT or RESOURCE	SOURCE	IDENTIFIER
MK2-IN-1	MCE	Cat# HY-12834
Ethidium Homodimer-I (EthD-I)	US Everbright	Cat# E4052
Lipofectamine 2000	Thermo Fisher Scientific	Cat# 11668019
SytoxGreen	Invitrogen	Cat# S34860
Cycloheximide (CHX)	MCE	Cat# HY-12320
NP-40 Lysis Buffer	Beyotime Biotechnology	Cat# P0013F
Protein A/G beads	Santa Cruz Biotechnology	Cat# sc-2003
FD4	MilliporeSigma	Cat# 46944
Ac-YVAD-pNA	Beyotime Biotechnology	Cat# P9701
Ac-LEVD-pNA	Beyotime Biotechnology	Cat# P9714
PMA	MilliporeSigma	Cat# 79346
TNF- α	PeprTech	Cat# 300-01A
IL-1 β	PeprTech	Cat# 200-01B
Streptomycin	Sangon Biotech	Cat# A610494
Nec-1s	Selleck Chemicals	Cat# S8641
PF-3644022	Selleck Chemicals	Cat# S8224
Tergitol	MilliporeSigma	Cat# 15s9
<i>Salmonella-Shigella</i> agar plates	Hangwei	Cat# M0062
Paraformaldehyde	Servicebio	Cat# G1101

Critical commercial assays

LDH Assay Kit	Beyotime Biotechnology	Cat# C0017
Luminescent Cell Viability Assay Kit	Promega	Cat# G7570
Bradford protein assay kit	Beyotime Biotechnology	Cat# P0006
Human IL-1 β kit	Boster	Cat# EK0392
Mouse IL-1 β kit	Boster	Cat# EK0394
Dual Luciferase reporter assay kit	Promega	Cat# E1910

Deposited data

Original western data for figures	This paper; Mendeley Data	https://data.mendeley.com/ https://doi.org/10.17632/ffpxt24ydz.1
-----------------------------------	---------------------------	--

Experimental models: Cell lines

Caco-2	Deng et al. ¹⁹	N/A
<i>NLRP6</i> ^{-/-} Caco-2	Deng et al. ¹⁹	N/A
HeLa	ATCC	N/A
WT MEF	This paper	N/A
<i>Nlrp6</i> ^{-/-} MEF	This paper	N/A
WT BMDM	This paper	N/A
<i>Nlrp6</i> ^{-/-} BMDM	This paper	N/A
HEK293T	ATCC	N/A

Experimental models: Organisms/strains

Mouse: C57BL/6 (Wt) mice	The Laboratory Animal Center of Soochow University	N/A
C57BL/6 <i>Nlrp6</i> ^{-/-} mice	Cambridge-Suda Genome Resource Center	N/A

(Continued on next page)

Continued

REAGENT or RESOURCE	SOURCE	IDENTIFIER
Oligonucleotides		
siRNA targeting sequence: <i>Gsdmd</i> : GGUGAACAUCCGAAAGAUUTT	GenePharma	N/A
siRNA targeting sequence: Control: UUCUCCGAACGUGUCACGUTT	GenePharma	N/A
Recombinant DNA		
Plasmid: pcDNA3.1-Flag for all transient expression vectors	This paper	N/A
Flag-RIP3	This paper	N/A
Flag-TRAF2	This paper	N/A
Flag-TRAF6	This paper	N/A
Flag-TAK1	This paper	N/A
Flag-TAB1	This paper	N/A
Flag-IKK β	This paper	N/A
Flag-p65	This paper	N/A
Flag-NLRP6	Deng et al. ¹⁹	N/A
Software and algorithms		
IBM SPSS statistics 22	IBM	https://www.ibm.com/
GraphPad Prism 8	GraphPad software, inc.	http://www.graphpad.com
ImageJ	National Institutes of Health	https://imagej.nih.gov/ij

RESOURCE AVAILABILITY

Lead contact

Further information and requests for reagents may be directed to and will be fulfilled by the lead contact Rui Huang (hruisdm@163.com).

Materials availability

This study did not generate new unique reagents. Plasmids and cell lines are listed in the [key resources table](#) and available for use upon request to the [lead contact](#).

Data and code availability

- All data is available within the paper or [supplemental information](#). Original western blot images have been deposited at Mendeley and are publicly available as of the date of publication. The DOI is listed in the [key resources table](#). Microscopy data reported in this paper will be shared by the [lead contact](#) upon request.
- This paper does not report original code.
- Any additional information required to reanalyze the data reported in this paper is available from the [lead contact](#) upon request.

EXPERIMENTAL MODEL AND STUDY PARTICIPANT DETAILS

Animals

Mice were bred in ventilated cages under 12-hour light/dark cycles in specific pathogen-free (SPF) conditions and received sterile water and food *ad libitum*. All experiments were conducted with ten- to twelve-week-old male mice in accordance with the principles and procedures outlined in the National Institutes of Health Guidelines for the Care and Use of Laboratory Animals (NIH Guidelines) and were approved by the Animal Experimental Committee of Soochow University (Grant 2111270). The mice were euthanized by CO₂ from compressed gas cylinders and we complied with all ethical regulations. Mouse strains used and generated in this study are listed in the [key resources table](#).

Cell culture studies

The human colon carcinoma Caco-2 cell line, the human epithelial carcinoma HeLa cell line, the human embryonic kidney HEK293T cell line, the mouse bone marrow-derived macrophages (BMDMs) and the mouse embryonic fibroblasts (MEFs) were maintained in a 5% CO₂ environment at 37°C as described in the method details section below.

Bacterial strains

S. Typhimurium strain SL1344 was a gift from Professor Qian Yang (Nanjing Agricultural University, Nanjing, China) and used for all experiments in this study.

METHOD DETAILS

Cell preparation

Bone marrow cells isolated from WT and *Nlrp6*^{-/-} mice were cultured in complete RPMI 1640 medium (HyClone Laboratories, Logan, UT, USA) supplemented with 10% (vol/vol) heat-inactivated fetal bovine serum (FBS; Biological Industries, Kibbutz Beit-Haemek, Israel), 10 ng/ml of Macrophage Colony Stimulating Factor (M-CSF; PeproTech, Rocky Hill, NJ, USA) and 1% (vol/vol) penicillin-streptomycin (Beyotime Biotechnology, Shanghai, China). Nonadherent cells were removed on day 3 and adherent cells became mature BMDMs on day 7. WT and *Nlrp6*^{-/-} MEFs isolated from E13.5 embryos were grown in Dulbecco's Modified Eagle Medium (DMEM; HyClone Laboratories) containing 10% (v/v) heat-inactivated FBS (Biological Industries) and 1% (v/v) penicillin-streptomycin (Beyotime Biotechnology). WT Caco-2 cells (human colon carcinoma cell line) were a gift from Professor Weiqi He (Cambridge Suda Genome Resource Center, Soochow University, Suzhou, China). *NLRP6*^{-/-} Caco-2 cells were constructed in our previous work.¹⁹ HeLa cells (human epithelial carcinoma cell line) and HEK293T cells (human embryonic kidney cell line) purchased from the American Type Culture Collection (ATCC; Manassas, VA, USA). Caco-2, HeLa and HEK293T cell lines were grown in DMEM medium (HyClone Laboratories) containing 10% (vol/vol) heat-inactivated FBS (Biological Industries).

Bacteria preparation

On the day of experiments, overnight *S. Typhimurium* cultures were diluted in a ratio of 1:100 and agitated for a further another 3 h until reaching the late-logarithmic phase in Luria-Bertani (LB) medium (Hangwei, Hangzhou, China). Upon washing 3 times with sterile PBS (Sangon Biotech, Shanghai, China), bacterial numbers were estimated and adjusted based on the optical density at 600 nm absorbance and ready for the further experiments.

S. Typhimurium infection *in vitro*

Bacterial suspension was added to mammalian cells at a multiplicity of infection (MOI) as described in the figure legends. BMDMs were washed 3 times with sterile PBS (Sangon Biotech) at 30 min after infection and other cells were washed at 1 h post-infection to remove extracellular bacteria. Infected cells were subsequently cultured in RPMI medium or DMEM medium containing 10% (vol/vol) heat-inactivated FBS (Biological Industries) and 50 µg/ml gentamicin (Sangon Biotech) for 2 h. Afterward, cell culture medium was replaced with those containing 10% (vol/vol) FBS (Biological Industries) and 10 µg/ml gentamicin (Sangon Biotech). Samples were collected for further experiments at the indicated time points as described in the figure legends. When appropriate, cells were pretreated or treated with GW806742X (HY-112292, MCE, New Jersey, USA), NSA (HY-100573, MCE), GSK'872 (HY-101872, MCE), zVAD (C1202, Beyotime), Nec-1 (HY-15760, MCE), (5Z)-7-Oxozeaenol (b7443, ApeXBio, Houston, TX USA), SB239063 (HY-11068, MCE) and MK2-IN-1 (HY-12834, MCE) as described in the figure legends. To assess cell membrane permeability, Ethidium Homodimer-I (EthD-I; US Everbright, Suzhou, China) was used as previously described.²⁴

Plasmid, siRNA and Transfection experiments

Plasmid encoding RIP3, TRAF2, TRAF6, TAK1, TAB1, IKKβ or p65 was successfully constructed. Plasmid encoding NLRP6 was constructed in our previous work.¹⁹ The negative control siRNA (NC siRNA) and siRNA specific for *Gsdmd* were purchased from GenePharma (Shanghai, China). Cells were transiently transfected with plasmid or siRNA using Lipofectamine 2000 (Thermo Fisher Scientific, Waltham, MA, USA) according to the manufacturer's instructions.

Cell death and viability assays

Cells were seeded in 96-well plates and incubated with the *S. Typhimurium* suspension as described above. For cell death assay, lactate dehydrogenase (LDH) released in supernatant was measured with a LDH Assay Kit (C0017, Beyotime Biotechnology), and the percentage of dead cells was calculated according to the manufacturer's instructions. SytoxGreen (S34860, Invitrogen by Thermo Fisher Scientific) was used according to the manufacturer's instructions and the intensity was measured as previously described.⁴⁰ For cell viability experiment, intracellular ATP levels were detected using a Luminescent Cell Viability Assay Kit (G7570, Promega, Madison, WI, USA) according to the manufacturer's instructions.

Western blot analysis

Samples were prepared as previously described.³⁹ Briefly, the cells were collected in NP-40 Lysis Buffer (P0013F, Beyotime Biotechnology) containing phosphatase inhibitor (Roche) and EDTA-free protease inhibitor (Biosharp) and incubated on a rocker with ice for 30 min, then centrifuged at 12000 g/4°C for 15 min to obtain cell lysates. Cell lysates were boiled at 100°C for 5 min in 5×SDS loading buffer. Equivalent amounts of protein extracts were separated on SDS-PAGE and electroblotted onto PVDF membranes (MilliporeSigma, Burlington, MA, USA). The membrane was blocked and then probed with the corresponding primary antibodies at 4°C overnight. After incubating with

appropriated secondary antibodies at room temperature for 1 h, membranes were visualized by chemiluminescence and the intensity was calculated by ImageJ Launcher broken symmetry software program (NIH, Bethesda, MD, USA). For western blot quantification, phospho blots and total blots were normalized to the housekeeping gene GAPDH, α -Tubulin or β -actin, then look at the phospho/total ratio using the normalized values.

Protein stability assay

Overexpression and endogenous TAK1 protein degradation was analyzed by a protein stability assay. In brief, 293T cells transfected with expression vector for Flag-TAK1 and increasing doses of expression vector for His-NLRP6. MEFs were incubated with 100 μ g/ml the protein synthesis inhibitor cycloheximide (CHX, HY-12320). TAK1 protein levels were analyzed by Western blot analysis.

Immunoprecipitation and ubiquitination assay

For immunoprecipitation, 293T cells transfected with indicated plasmids were harvested and lysed with NP-40 Lysis Buffer (P0013F, Beyotime Biotechnology). Protein extracts were incubated with anti-Flag immunomagnetic beads (M8823, Sigma-Aldrich) at 4°C overnight. For ubiquitination assay, MEFs were harvested and lysed with NP-40 Lysis Buffer (P0013F, Beyotime Biotechnology). The supernatants were denatured at 95°C for 5 min in the presence of 1% SDS, then diluted with lysis buffer to reduce the concentration of SDS below 0.1% and incubated with TAK1 antibody (12330-2-AP, Proteintech) plus Protein A/G beads (sc-2003, Santa Cruz Biotechnology) at 4°C overnight. The immune complexes were then analyzed by Western blot analysis.

TEER and epithelial permeability assay

WT and *NLRP6*^{-/-} Caco-2 cells were seeded in Transwell inserts (3 μ m pore size, Corning, NY, USA) for up to 14–21 days. The TEER was measured using a Millicell Electrical Resistance System (Millicells Voltmeter, MilliporeSigma) to monitor the monolayer integrity. A TEER value of at least 200 Ω /cm² was used for below experiments.⁴¹ The bacterial suspension was added to the apical side of the Transwell system at the MOI of \sim 100. TEER was measured every 0.5 h. For bacterial translocation, the culture medium was collected from the basal well at 3 h post-infection, and then translocated bacteria were enumerated by plating. Epithelial permeability was measured by apical-to-basal transport of FD4 (46944, MilliporeSigma). Bacteria resuspended in DMEM containing 10% (vol/vol) FBS (Biological Industries) and 5 mg/ml FD4 were added to the apical side of the Transwell system at the MOI of \sim 100. At 3 h post-infection, the culture medium was collected from the basal well. The fluorescence was measured at an excitation wavelength of 485 nm and an emission wavelength of 520 nm.

Caspase substrate cleavage assay

Cells were lysed with caspase assay buffer and mixed with Ac-YVAD-pNA (P9701, Beyotime Biotechnology) or Ac-LEVD-pNA (P9714, Beyotime Biotechnology) according to the manufacturer's instructions. OD values were read at 405nm. Total protein content was measured using a Bradford protein assay kit (P0006, Beyotime Biotechnology) according to the manufacturer's instructions. The cleavage activity was normalized to the protein concentration of each sample.

ELISA

The production of cytokines was detected with human IL-1 β kit (EK0392, Boster) and mouse IL-1 β kit (EK0394, Boster) according to the manufacturer's protocols.

Luciferase reporter assays

HEK293T cells were seeded at a density of 5 x 10⁴ cells per well in 24-well plates overnight. Cells were then transfected with the experimental reporter plasmid pNF- κ B-Luc (Firefly luciferase, Clontech, Mountain View, CA, USA), pIL8-Luc and the internal control plasmid pRL-TK (Renilla luciferase, Clontech), as well as other plasmids as described in the figure legend and our previous study.⁴² When appropriate, cells were treated with PMA (79346, MilliporeSigma), TNF- α (300-01A, PeproTech) or IL-1 β (200-01B, PeproTech). Enzyme activity was measured using the Dual Luciferase reporter assay kit (E1910, Promega) according to the manufacturer's instructions.

Mouse experiments and ethics statement

WT mice (C57BL/6) were purchased from the experimental animal center of Soochow University. *Nlrp6* knockout mice on the C57BL/6 genetic background was a gift from Professor Ying Xu (Cambridge-Suda Genome Resource Center, Soochow University, Suzhou, China). To establish bone marrow chimeras, WT and *Nlrp6*^{-/-} mice were lethally irradiated with 8 Gray using a cesium source. Recipient mice were reconstituted intravenously with 8 million bone marrow cells derived from healthy donor mice at 3 h post irradiation, and then kept under 0.2% neomycin sulfate treatment via the drinking water, *ad libitum*, for 2 weeks. 8 weeks after transplantation, the chimeric mice were ready for the further experiments.

A model of oral *S. Typhimurium* infection was established as previously described.⁴³ In brief, mice orally treated with 20 mg/mouse streptomycin (Sangon Biotech) for 24 h and then orally administrated with *S. Typhimurium* strain SL1344. When appropriate, mice were treated with the RIP1 inhibitor Nec-1s (S8641, Selleck Chemicals, Houston, TX, USA) or the MK2 inhibitor PF-3644022 (S8224, Selleck Chemicals). To determine the viable counts of *S. Typhimurium*, MLN, liver and spleen were harvested aseptically, weighed, and homogenized in 4°C PBS

containing 0.5% (vol/vol) Tergitol (15s9, MilliporeSigma) and 0.5% (vol/vol) FBS (Biological Industries). Bacterial burden was determined in appropriate dilutions by plating on *Salmonella-Shigella* agar plates (M0062, Hangwei). Ileum, colon and spleen samples were fixed in 4% paraformaldehyde (Servicebio, Wuhan, China), embedded in paraffin and cut into 5- μ m thick sections. The sections were then incubated with p-MLKL antibody (ab196436, Abcam) according to the manufacturer's instructions. Photomicrographs were taken with a Nikon Eclipse Ni-U fluorescence microscope (Nikon Corporation, Tokyo, Japan) with NIS-Elements F (Nikon Corporation). Ileal and colonic IECs were isolated as previously described and western blot analysis was performed as described above.⁴⁴ To assess intestinal permeability, mice were orally gavaged with FD4 (12 mg per mouse; MilliporeSigma) 4 h prior to sacrifice. Serum samples were collected, and fluorescence was measured at an excitation wavelength of 485 nm and an emission wavelength of 520 nm.

QUANTIFICATION AND STATISTICAL ANALYSIS

Data are presented as mean \pm SEM. Statistical analysis was performed using IBM SPSS statistics 22 (Chicago, IL, USA). Normality of numerical variables was assessed and in the case of normality. Comparisons of 2 groups were analyzed using an independent Student's t test. Values of $p < 0.05$ were considered statistically significant.